3

Silicon Oxide (SiO_x, 0<x<2): a Challenging Material for Optoelectronics

Nicolae Tomozeiu
R&D Department, Océ Technologies B.V., The Netherlands

1. Introduction

1.1 Why SiO_x in optoelectronics

A complete integration of the silicon based optoelectronic devices was not possible, for many decades, to be made because the silicon is an inefficient emitter of light. Being a semiconductor with an indirect band-gap and having efficient free carrier absorption of the radiation, the crystalline silicon was considered an inadequate material for light emitter diodes (LED) and laser diodes to produce totally integrated optoelectronic devices. In the last two decades, special attention has been paid to the light-emission properties of low-dimensional silicon systems: porous silicon (Cullis & Canham, 1991; Wolkin et al., 1999), super-lattices of Si/SiO_2 (Zu et al.,1995), silicon nano-pillars (Nassiopoulos et al., 1996), silicon nanocrystals embedded in SiO_2 (Wilson et al., 1993) or in Si_3N_4 (Cho et al., 2005). Both, the theoretical understanding of the physical mechanisms (quantum confinement of excitons in a nano-scale crystalline structure) and the technological advance to manufacture such structures have paved the path to produce a silicon based laser.

Pavesi at al (2000) have unambiguously observed modal and net optical gains in silicon nanocrystals. They have compared the gain cross-section per silicon nano-crystal with that the one obtained with A_3B_5 (e.g. GaAs) quantum dots and it was found orders of magnitude lower. However, owing to the much higher stacking density of silicon nanocrystals with respect to direct band-gap A_3B_5 quantum dots, similar values for the material gain are observed. In this way, the route towards the realization of a silicon-based laser, and from here, of a highly integrated silicon based optoelectronic chip, is open.

The silicon nano-crystals (Si-nc) embedded in various insulators matrix have been intensively studied in the last decade. Either the photoluminescence (PL) properties of the material or the emitted radiation from a LED/ diode laser structure was studied. A clear statement was made: the peak position of PL blue-shifts with decreasing the size of Si-nc. The nano-crystals interface with the matrix material has a great influence on the emission mechanism. It was reported that due to silicon-oxygen double bonds, Si-nc in SiO_2 matrix has localized levels in the band gap and emits light in the near-infrared range of 700–900 nm even when the size of Si-nc was controlled to below 2 nm (Wolkin et al., 1999; Puzder et al., 2002).

In the last decades, silicon suboxides (hydrogenated and non-hydrogenated) have been proposed as precursors for embedded silicon nano-crystals into silicon dioxide matrix. This material is a potential candidate to be used in laser diodes fabrication based on silicon technology. The need for such device was (and is) the main reason for theoretically (ab initio

theories) and experimentally investigations of SiO_x. This chapter dedicated to silicon suboxide as a challenging material for silicon based optoelectronics, begins in section two with a small (but comprehensive) discussion on the structural properties of this material. The implications of the SiO_x composition and its structural entities on the phonons' vibrations are shown in the third section. Here are revealed the IR spectra of various compositions of the SiO_x thin films deposited by rf reactive sputtering and the fingerprints related to various structural entities. The electronic density of states (DOS) for these materials is the subject of the forth section. Here are defined the particularities of the valence- and conduction band with special attention to the structural defects as silicon dangling bonds (DB). Having defined the main ingredients to understand the optical and electrical properties of the SiO_x layers, these properties are discussed in the fifth and the sixth section, respectively. The investigations and their results on as deposited SiO_x materials are analyzed in this section. In the first part of this introduction it was mentioned that the material for optoelectronics is the silicon nano-crystals embedded in SiO_2. The physical processes in order to obtain the silicon nano-particles from SiO_x thin films are presented in section seven. The phase separation realized with post-deposition treatments as thermal annealing at high temperature, or ion bombardment or irradiation with UV photons is extensively discussed. This section ends with a brief review of the possible applications of the Si-nc embedded into a dielectric matrix as optoelectronic devices. Of course the main part is dedicated to the silicon-based light emitters.

2. The structure of SiO_x (0<x<2)

2.1 Introductive notions

The structure of the silicon oxide, as the structure of other silicon-based alloys, is build-up from tetrahedral entities centered on a silicon atom. The four corners of the tetrahedral structure could be either silicon or oxygen atoms. Theoretically, this structural edifice appears as the result of the "chemistry" between four-folded silicon atoms and two-folded oxygen atoms, developed under specific physical conditions. It is unanimously accepted that an oxygen atom is bonded by two silicon atoms and never with another oxygen atom. The length of the Si-O bond is 1.62 Å while the Si-Si bond is 2.35 Å. The dihedral anglebetween two Si-Si bonds (tetrahedron angle) is 109.5^0 and the angle formed by the Si-O bonds in the Si-O-Si bridge is 144^0. These data are the results of dynamic molecular computation (Carrier et al., 2002) considering the structure completely relaxed. In reality, the structure of the SiO_x thin films deposited by PVD or CVD techniques is more complicated. Both the bond length and the dihedral angle vary. Moreover, the picture of the structural design is complicated because the Si-O bond is considered partially ionic and partially covalent (Gibbs et al., 1998).

2.2 SiO_x structure: theoretical assumptions

In order to obtain an elementary image of the SiO_x structure, we use a simple model. It is important to evaluate the main elements that define the material structure: the energy involved in keeping together the atoms within a specific structure and the number of each atom species from a defined alloy. The Si–Si and Si–O bonds are characterized by dissociation energy of 3.29 eV/bond and 8.26 eV/bond, respectively (Weast, 1968). The particles' density in crystalline silicon (c-Si) is $5 \cdot 10^{28}$ m^{-3} while for crystalline quartz (c-SiO_2) is $6.72 \cdot 10^{28}$ m^{-3}. Interpolating, it can be found for SiO_x:

$$N_{SiO_x}^{at} = 5 \cdot 10^{28} + 8.55 \cdot 10^{27} \cdot x \quad (m^{-3}), \tag{1}$$

where x=O/Si.
The silicon atoms' density is:

$$N_{Si} = N_{SiO_x}^{at} \cdot \frac{1}{1+x} \tag{2a}$$

and the oxygen atoms' density is:

$$N_O = N_{SiO_x}^{at} \cdot \frac{x}{1+x} \tag{2b}$$

Taking into account the fact that the silicon atom is four-coordinated and the oxygen is two-coordinated, the number of bonds can be easily calculated:

- O atoms are involved in Si–O–Si bridges[1], which means two Si-O bonds: n(Si–O–Si) = 2 ·n (Si–O) = N_O (one oxygen atom contributes to two Si-O bonds);
- Si atoms will contribute to Si–Si and Si–O–Si bonds: n(Si–Si, Si–O–Si)=(4/2) ·N_{Si}, (one silicon atom is shared by 4 Si-Si and/or Si-O bonds and it must be considered only once);

This means that for Si – Si bonds it is easy to write: n(Si–Si)= n(Si–Si, Si–O–Si) – n(Si–O–Si), where n(A -B) is the number of bonds between atom specie A and atom specie B from an AB alloy, while N_y, with y=Si, O is the number of specie "y" atoms.
Having the number of bonds and the energy per bond, the energy involved in a SiO_x material can be estimated. This represents practically the necessary energy to break all bonds between the atoms that form a structural edifice. Following the calculations presented above, the density of Si–Si and Si–O bonds versus silicon suboxide composition (x parameter from SiO_x) is shown in figure 1a. Also, the values of the SiO_x density energy (in J/m^3) calculated for x ranging between 0 and 2 are displayed in figure 1b. The latter is an important parameter for experiments considering the structural changes of an already deposited (grown) SiO_x material.

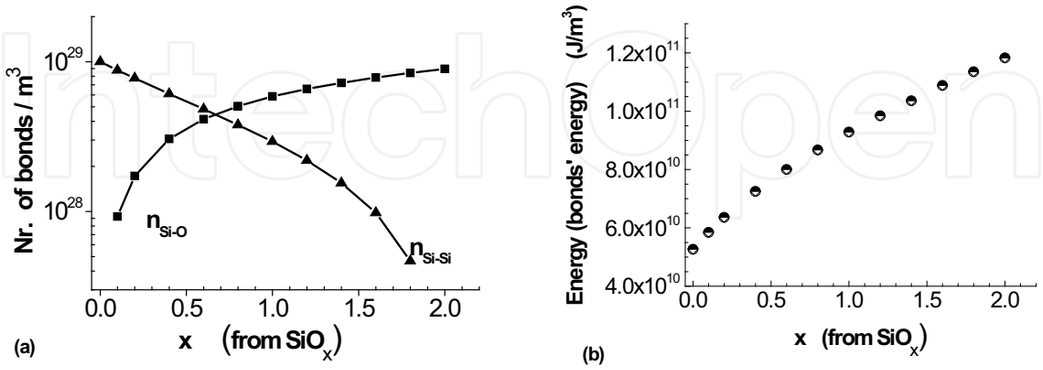

Fig. 1. (a) The calculated values of the Si-Si and Si-O bonds density as a function of x; (b) the dissociation energy per volume unit versus x parameter.

[1] The number of O-O bonds is considered as being equal to zero.

The interpretation of the data presented in figure 1b, is simple: for a sample with certain x value, if the corresponding value of the dissociation energy is instantaneously delivered, we can consider that for an extremely short time, the bonds are broken and the atoms can "look for" configurations thermodynamically more stable. With short laser pulses, such kind of experiments can be undertaken and structural changes of the material can be studied.

2.3 The main SiO_x structural entities

Varying the number of oxygen atoms bonded to a silicon atom considered as the center of the tetrahedral structure, five entities can be defined. In a simple representation they are shown in figure 2. For a perfect symmetric structure (the second order neighboring atoms included), the Si–Si distance is 1.45 times the Si–O length. The nature of the Si–O bond makes the pictures shown in figure 2 more complicated. The electrical charge transferred to the oxygen neighbor charges positively the silicon atom. This means that a four-coordinated silicon can be noted as Si^{n+} where n is the number of oxygen atoms as the nearest neighbors. The length of a Si–Si or Si–O bond, as well as the angle between two adjacent bonds, is influenced by the n+ value and the spatial distribution of those n oxygen atoms around the central silicon atom. Of course the 4-n silicon atoms are also Si^{m+} like positions and they will influence the length of the Si^{n+} - Si^{m+} bond. Using first-principles calculations on Si/SiO_2 super-lattices, P. Carrier and his colleagues (Carrier et. al., 2001) have defined the interfaces as being formed by all Si^{1+}, Si^{2+} and Si^{3+} entities. The super-lattice structure has been considered within a so-called *fully-relaxed model*. The main outcome of these calculations is that the bond-lengths of partially oxidized Si atoms are modified when compared with their counterparts from Si and SiO_2 lattice. As examples we mention: within a Si^{1+} structure the Si^{1+} – Si^{m+} bond is 2.39 Å for m=2 and 2.30 Å when m=0. The Si^{n+} - O has a length of 1.65Å when n=1 and 1.61 Å for n=3. All these have influences on the structural properties of the material and from here on the density of states assigned to the phonons and electrons. The influence on physical properties (electrical, optical and mechanical) of the material deposited in thin films will be discussed in the next sections.

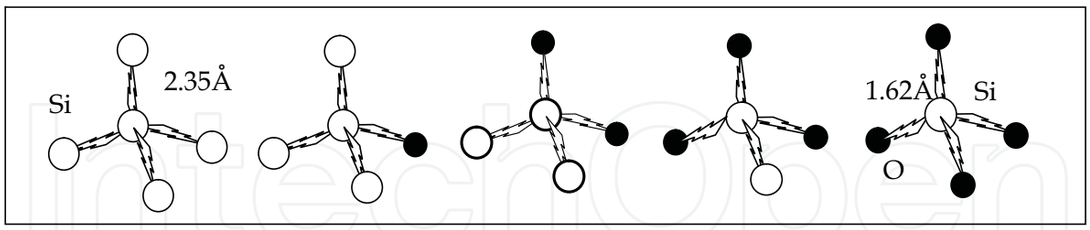

Fig. 2. The five structural entities defined as Si^{n+} in SiO_x alloys. The structures are build-up around a central Si atom from n oxygen atoms (the filled circles) and 4-n silicon atoms (empty circles)

It should be noted that the differences in both the bond length and the dihedral angle of two adjacent bonds determine, for each structural entity, small electrical dipole with great impact on properties as electrical conductivity and dielectric relaxation. A contribution of the polarization field on the local electrical field will determine hysteresis – like effects, that could be used in some applications.

The multitude of possible connexions between various structural entities defines on macroscopic scale a SiO_x structure full of mechanical tensions which, speaking from a

thermodynamic perspective, provides an unstable character to the material. It is easy to see that a material formed from Si^{0+} or Si^{4+} structures without defects (e.g. dangling bonds) is thermodynamically stable.

3. The phonons' vibrations and SiO_x structure

3.1 Phonons' and molecular vibrations

Within the so-called Born – Oppenheimer adiabatic approximation, the general theory of solid state physics shows that the movement of the light particles-component of atoms (electrons) can be neglected or considered as a perturbation for the movement of the heavy parts of the atom (ions). In these conditions, for a crystalline material, the Schrödinger equation assigned to the system of heavy particles is:

$$\hat{H}_z \Psi\left(\left\{\vec{R}_\alpha\right\}\right) = E\Psi\left(\left\{\vec{R}_\alpha\right\}\right) \tag{3}$$

where the Hamiltonian $\hat{H}_z$ is a sum of three terms:

i. the first one describes the kinetic energy: $\sum_\alpha \left(\frac{P_\alpha^2}{2M_\alpha}\right)$, with α the number of particles, M_α and P_α- the mass and the momentum of the ion;

ii. the second one : $\frac{1}{2}\sum_{\alpha,\beta(\alpha\neq\beta)} \hat{V}_{\alpha\beta}$ is the potential energy due to the interaction between ions;

iii. and the third one defined as $\hat{E}_e\left(\left\{\vec{R}_\alpha\right\}\right)$ represents the electrostatic interaction between ions and electrons.

The equations (3) have been solved considering that the lattice vibrations involve small displacement from the equilibrium position of the ion: 0.1 Å and smaller. Under the so-called harmonic approximation, the problem is seen as a system of quantum oscillators with the solution:

- the eigenvector Ψ was found as

$$\Psi = \prod_\alpha \psi_\alpha \tag{4}$$

with $\psi_\alpha = \frac{\exp\left(i\vec{k}\vec{R}_\alpha\right)}{\sqrt{V}} \cdot u_{\alpha\vec{k}}(\vec{R}_\alpha)$ given by the Bloch functions.

- the eigen-values for energy:

$$E = \sum_\alpha E_\alpha = \sum_\alpha h\nu_\alpha \cdot \left(N_\alpha + \frac{1}{2}\right) \tag{5}$$

The relation (5) shows that $h\nu_\alpha$ is a quantum of energy assigned to the lattice oscillation. It represents the energy of a *phonon* – quasi-particle that describes the collective movement of the lattice constituents. The phonons are characterized by energy and momentum (impulse)

as long as the lattice and the collective movement of the atoms (ions) exists. Only under these conditions, the phonon can be understood as a particle that can interact with other particles (e.g. electrons, photons).

Let us consider a molecule formed from different atoms where the bond lengths and the bond angles represent the average positions around which atoms vibrate. At temperatures above absolute zero, all the atoms in molecules are in continuous vibration with respect to each other. If the molecule is consisting of N atoms, it has a total of 3N degrees of freedom. For nonlinear molecules, 3 degrees of freedom describe the translation motion of entire molecule in mutually perpendicular directions (the X, Y and Z axes) and other 3 degrees correspond to rotation of the entire molecule around these axes. For a linear molecule, 2 degrees are rotational and 3 are translational. The remaining 3n-6 degrees of freedom, for nonlinear molecules, respectively 3n-5 degrees for linear molecules are *fundamental vibrations*, also known as *normal modes of vibration*.

Considering the adiabatic approximation and harmonic displacements of the atoms from their equilibrium positions, for each vibrational mode, q, all the atoms vibrate at a certain characteristic frequency, ν_q called *fundamental frequency*. In this situation, for any mode the vibration energy states, $E_{q\nu}$, can be described by:

$$E_{q\nu}^{harm} = h\nu_q\left(n_q + \frac{1}{2}\right) \tag{6}$$

where h is Planck's constant, n_q is the vibrational quantum number of the q-th mode (n_q=0, 1, 2, …). The ground state energy (that corresponds to $n_q = 0$) is $h\nu_q/2$ and each excited state, defined by the vibrational quantum number has an energy defined by the Rel. (6). The energy difference for transitions between two adjacent states is constant and equals $h\nu_q$.

The theoretical model of the harmonic displacement of the atoms helps to easily describe the atoms movement. In reality, the structural edifice of the molecule supposes atoms that belong to intra-molecule bonds or to inter-molecules bonds. This means that the character of harmonic oscillator disappears and a molecule is in fact an anharmonic oscillator. Introducing an anharmonicity parameter γ_q for each vibrational mode, the phonon energy can be expressed as:

$$E_{q\nu} = E_{q\nu}^{harm} + h\nu_q\gamma_q\left(n_q + \frac{1}{2}\right)^2 \tag{7}$$

where γ_q is dimensionless.

How the length of the bond (the interatomic distance) influences the phonon energy?

Considering a di-atomic molecule, its potential energy as a function of the distance between the atoms within an anharmonic oscillation is suggestively shown in figure 3. The minimum in the potential energy is reached when the distance between the two atoms equals the "bond length". As the inter-atomic distance increases, the potential energy reaches a maximum, which defines the bond dissociation energy.

An interesting observation is that the energy levels of the oscillator which represents the diatomic molecule are quantified (they have discrete values) and they become closer with increasing the interatomic distance. This means that the needed energy to excite the phonon on the nearest energy state, $h\nu_q$, is smaller when the distance between the atoms increases.

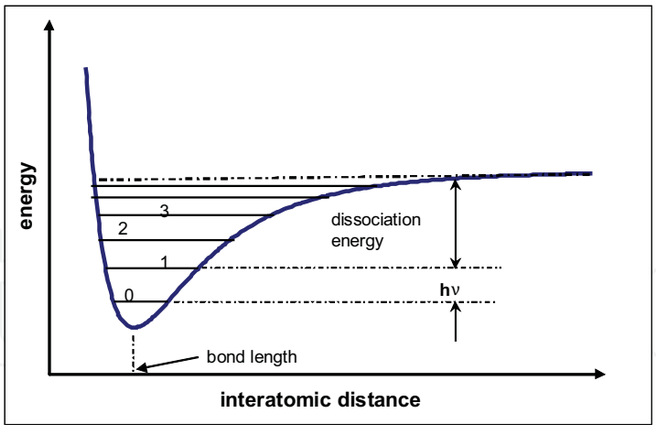

Fig. 3. The potential energy for a di-atomic molecule versus the interatomic distance, within the anharmonic oscillation model.

How the mass of the two atoms influences the phonon frequency? To answer this question, let's consider the simplest oscillator (a mechanical spring connecting two masses) and apply the classical Hooke's law. If m_1 and m_2 are the mass values for the two atoms, the frequency oscillation is:

$$\nu = \frac{1}{2\pi} \cdot \sqrt{\frac{k}{\mu}} \tag{8}$$

with the reduced mass, μ, given by $\mu = \frac{m_1 m_2}{m_1 + m_2}$. The parameter k is called the elastic force constant of the bond and it defines the bond strength.

In most books of the IR spectroscopy the oscillation frequency is given in wave-number unit that is the inverse of the wavelength. In this condition the Rel. (8) becomes

$$\tilde{\nu} = \frac{1}{\lambda} = \frac{1}{2\pi c} \cdot \sqrt{\frac{k}{\mu}} \quad (\text{cm}^{-1}) \tag{8'}$$

with c the speed of light, $3 \cdot 10^{10}$ cm/s. Therefore, for the heavier atoms the vibration frequency is smaller. However the strength of the bond is also defining the vibrational frequency. In other words, the nature of the bond is important. We can conclude that the phonon spectrum is specific to each type of molecule and it could be utilized in identification of the atomic species.

We note that, within a multi-atomic molecule, the motion of two atoms cannot be isolated from the motion of the rest of the atoms in the molecule. Also, in such a molecule, two oscillating bonds can share a common atom. When this happens, the vibrations of the two bonds are coupled.

3.2 IR active vibrations - a theoretical approach

IR spectroscopy is one of the most utilized techniques in analyzing the compositional and structural properties of a molecular compound. When a radiation of IR optical range, with

energy hν, is sent on a molecular system whose vibration frequency is ν, that radiation is absorbed, if the molecule has electrical dipole.
As a result of the interaction between the electrical field of the IR electromagnetic wave and the molecular dipole, the molecule will make a transition, in energy, between the states "i" and "j". The *transition moment* $\Im$ is defined by:

$$\Im = \int \psi_i^* \mu \psi_j d\tau \tag{9}$$

where ψ and ψ* are the eigen-function and its complex conjugate; dτ is the integration over all space. In the relation (9) μ is the *dielectric dipole moment* defined as:

$$\mu = q \cdot r \tag{10}$$

with q the charge of the dipole and r the distance between the charges.
Taking into account the vibrational motion of the atoms, the dielectric dipole changes, because the distance r changes:

$$\mu = \mu_0 + (r - r_e) \cdot \left(\frac{\partial \mu}{\partial r}\right)_0 + \frac{1}{2} \cdot (r - r_e)^2 \cdot \left(\frac{\partial^2 \mu}{\partial r^2}\right)_0 + \ldots$$

In this situation the transition moment becomes:

$$\Im = \int \psi_i^* \left[\mu_0 + (r - r_e) \cdot \left(\frac{\partial \mu}{\partial r}\right)_0 \right] \psi_j \cdot d\tau \tag{11}$$

When μ_0 is a constant, because of the orthogonality of the eigen-functions, ($\int \psi_i^* \psi_j \, d\tau = 0$), the relation (11) remains:

$$\Im = \int \psi_i^* \left[(r - r_e) \cdot \left(\frac{\partial \mu}{\partial r}\right)_0 \right] \psi_j \cdot d\tau \tag{12}$$

The transition probability is defined as $\Im^2$, and it scales the radiation absorption. With other words, the intensity of the IR absorption peak is proportional to the square of $\Im$ and $\left(\frac{\partial \mu}{\partial r}\right)$. We can say that the *molecules with* $\left(\frac{\partial \mu}{\partial r}\right) = 0$ *are IR inactive* because the absorption of the radiation is zero. We note that molecule with small dipole moment μ may have large $\left(\frac{\partial \mu}{\partial r}\right)$ and vice-versa. In both situations, according to Rel. (12), absorbing bands will appear in the IR spectrum.
Therefore, we can conclude that among the fundamental vibrations, those that produce a change in the dipole moment may result in an IR activity. Certain vibrations *give polarizability changes and they may give Raman activity*. Some vibrations can be both IR- and Raman-active.

3.3 The IR fingerprints of the SiO_x structural entities

Does the SiO_x structure have an electrical dipole to interact with the incident IR radiation and to release an IR absorption spectrum?

Considering the structural entities presented in figure 2, all entities that contain at least one oxygen atom have such an electrical dipole. The tetrahedral structure build up around a silicon atom by its four neighbors will have a certain asymmetry concerning the "gravity center" of the positive charge vis-à-vis of that the one of the negative charge. By molecular vibration a dipole is generated and, according to the theoretical explanation given in the previous section, energy of the IR electromagnetic field will be absorbed.

Calculations based on theoretical models (simpler or more sophisticated, modern) have produced the local density of vibrational states (LDOVS) for Si and O atoms (Lucovski and Pollard, 1963, Knights et al., 1980, Pai et al., 1986). The IR absorption spectrum specific to a SiO_2 structure was calculated taking into account these LDOVS' and as it can be seen in figure 4 (after P.G. Pai et al., 1986) there are three vibrational bands which correspond to rocking, bending and stretching motions of the oxygen atoms. As a first observation, the dominant calculated peak in the IR absorption spectrum of SiO_2 is associated with stretching motion of the oxygen atoms. The peak position and the shape of the peak absorption are greatly affected by the mixing of Si and O atoms.

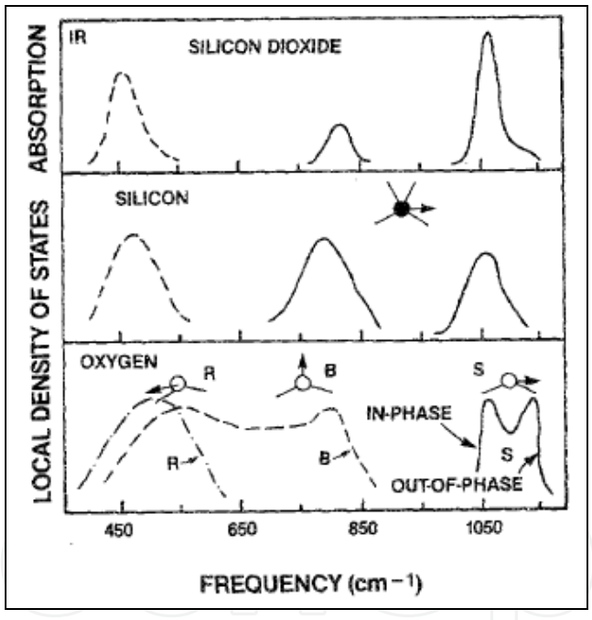

Fig. 4. Local density of vibrational states (LDOVS) for oxygen and silicon and, calculated IR response for silicon dioxide. *Reprinted with permission from Pai et al., 1986; copyright 1986, American Vacuum Society.*

According to the model proposed by Pai and his colleagues (Pai et al., 1986), this peak is an interesting example of coupled oscillations: the motion of the oxygen atom and that of the neighboring silicon atoms. The low frequency part of the spectrum peak is "imposed" by the silicon atoms' vibration (the motion of the oxygen atom is in phase). The high frequency edge of the same peak is dominated by oxygen; there is a little associated silicon motion, which is out of phase motion compared with the movement of the oxygen atoms. A broad shoulder centered at about 1150cm^{-1} generally gives this part of the peak.

The IR vibrations of a Si–O–Si entity belonging to the SiO_x structure are briefly presented as following:

- a bond-stretching vibration, ν_s, in which the O displacement is in a direction parallel to the line joining its neighboring silicon (in a-Si matrix, the peak absorption is placed at 940cm^{-1} and in thermally growth a-SiO_2 is at 1073cm^{-1});
- bond-bending vibration, ν_B, in which the O atom motion is along the bisector direction of the Si-O-Si bond angle (ν_B=780cm^{-1});
- out of plane rocking motion, ν_R, with ν_R=450cm^{-1}.

The majority of the published papers reveal the particularities of the stretching vibration peak. The oxygen atom is bonded to two adjacent silicon atoms by Si–O bonds. Considering the diatomic model described in the previous section, the movement of the oxygen atom is the result of the coupling of the two Si–O vibrations. The strength of the bond and the vibration frequency are dependent not only on the Si and O atoms partners in the bond, but also on the other neighbors of the silicon atom. Schematically, the Si–O–Si bridge is shown in figure 5.

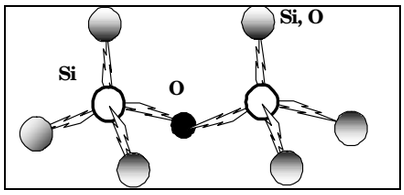

Fig. 5. A sketch of the Si–O–Si structural bridge with the other 6 atoms neighboring the two silicon atoms, which can be either oxygen atoms or silicon.

A measured IR spectrum of a SiO_x thin film deposited by reactive rf sputtering is shown in figure 6. The thickness of the layer was determined as being d=620nm and the composition corresponds to x=0.73. The rocking, bending and stretching modes of Si-O-Si are identified.

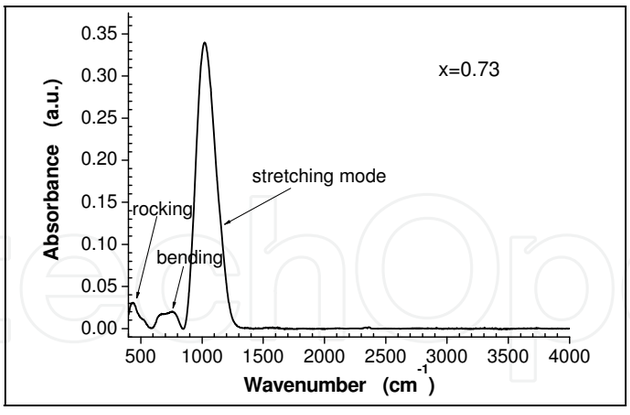

Fig. 6. The IR spectrum of SiO_x layer with x=0.73.

The peak position and the shape of the absorption peak assigned to the stretching vibration mode depend on the composition. This is well revealed in figure 7 where the normalized spectra are shown for SiO_x samples with x between 0.1 and 2. Increasing the oxygen content, the main peak position shifts towards larger wavenumber values, while its width becomes smaller. For larger x values, (x>1.2), a shoulder appears on the 1150 cm^{-1}, which becomes more and more pronounced when the oxygen content increases. For x=2 this shoulder is a characteristic feature for the SiO_2 structural entities.

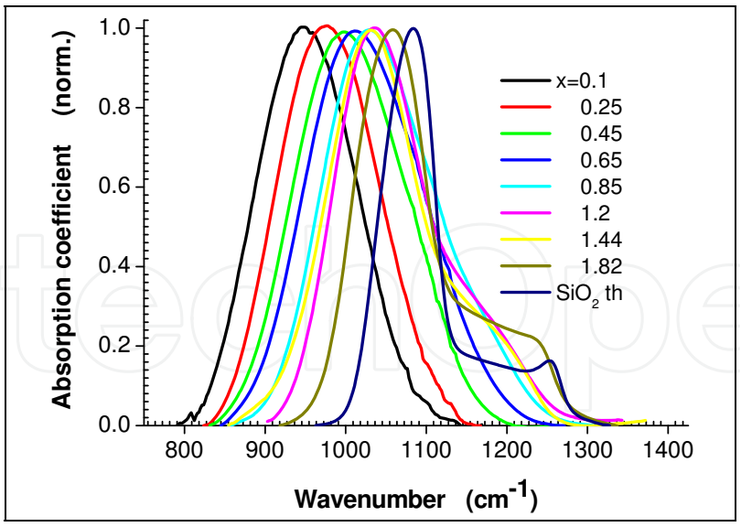

Fig. 7. The position and the shape of the absorption peak assigned to the stretching vibration mode of the Si–O–Si bridge are dependent on the oxygen content.

The shift in the peak position could be used to scale the oxygen content. This is applied when the samples have been deposited with the same technique, with well defined deposition conditions. A calibration curve between the oxygen content previously determined via other techniques (Rutherford back-scattering, or x-ray photoelectron spectroscopy, etc) and the IR peak position is needed. It must be mentioned that, although this method to determine the layer composition is used in many labs, the peak position is dramatically influenced by the deposition conditions (Tomozeiu, 2006). There is another model to determine the oxygen concentration from IR absorption measurements using the integrated absorption of the stretching mode peak. Also here, it is necessary to calibrate the method. This means that for some samples, the x parameter must be determined via other methods. The IR spectroscopy is set as a secondary standard in measuring the oxygen content.

The method was proposed by Zacharias and his colleagues to determine the concentrations of hydrogen and oxygen in a-Si:O:H thin films (Zacharias et al., 1994). It is based on the aria of the IR absorption peak related to that atomic species and the connection with the concentration is:

$$c(i) = A(i) \int_{\tilde{\nu}_{peak(i)}} \frac{\alpha(\tilde{\nu})}{\tilde{\nu}} d\tilde{\nu} \tag{13}$$

where c(i) is the concentration of element i (H or O), $\alpha(\nu)$ is the absorption coefficient in the peak region centered on $\tilde{\nu}_{peak}$ and $A(i)$ is the calibration factor. Writing this formula for SiO_x, the oxygen concentration is: c(O)=A(O)*I(1080-960), where I(1080-960) is the integrated absorption between $\tilde{\nu}$ =960 cm^{-1} and $\tilde{\nu}$ =1080 cm^{-1}.

For the spectra presented in figure 7 the calculated values of the integrated IR absorption are shown in figure 8. A good linearity between the integrated absorption and the x values is found for x<1.3. For samples with oxygen content higher than the value corresponding to this point, there is a rapid increase of the integrated IR absorption. In other words, at x=1.3 there is a kink point (Tomozeiu et al., 2003) in the plot shown in figure 8. This was evaluated as a signal that the SiO_x structure changes from a random distribution of the Si–O bonds in

the material bulk (RBM model) to a random mixing model (RMM) which describes the material in terms of domains of fully oxidized silicon (SiO_2) and low-oxygen silicon. Similar results have been reported by F. Stolz and his colleagues (Stolz et al., 1993) on SiO_x samples prepared under other conditions than those investigated in the figure 7. For the data presented in figure 8, the relation (13), in terms of x parameter, becomes:

$$x = 5.49 \cdot 10^{-4} \cdot I(1080 - 960), \qquad \text{with } x < 1.3 \tag{13'}$$

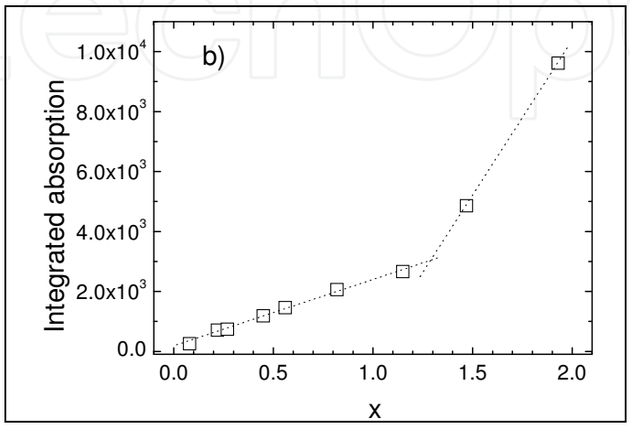

Fig. 8. The integrated IR absorption of the stretching mode near 1000 cm^{-1} versus the SiO_x oxygen content. A kink point is outstanding near x=1.3

3.4 The material structure reflected in the IR absorption spectrum

Is the first part of the plot from figure 8 describing the SiO_x structure based on a random bonding model (RBM)?

The answer is based on a simpler theoretical model proposed by A Morrimoto and his colleagues (Morimoto et al., 1987). They assumed a random distribution of the *Si-O-Si* bonds and they calculated the probability that "*n*" oxygen atoms will neighbor a *Si-O-Si* bridge.

The probability to have "*n*" O-atoms and "6-n" Si-atoms around the *Si-O-Si* bridge (see the figure 6) is:

$$P_n(x) = C_6^n P(Si)^{6-n} P(O)^n \qquad n = 0 \div 6 \tag{14}$$

where C_6^n gives the number of arrangements in which n sites are chosen from the total of 6 sites, *P(Si)* and *P(O)* being the presence probability of *Si* and *O*, respectively.

Considering the number of *Si-Si* bonds and the number of *Si–O* bindings as a function of the oxygen content, (see section 2.2) the *P(Si)* and *P(O)* probabilities are easy to calculate:

$$P(Si) = \frac{n(Si-Si)}{n(Si-Si, Si-O-Si)} = 1 - \frac{x}{2} \tag{15a}$$

and respectively:

$$P(O) = \frac{n(Si-O-Si)}{n(Si-Si, Si-O-Si)} = \frac{x}{2}. \tag{15b}$$

In this way, the probability to have the richest in silicon SiO_x is given by Rel. (14) with n=0: $P_0(x)=\left(1-\frac{x}{2}\right)^6$ and the probability to have the richest in oxygen SiO_x is obtained for n=6: $P_6(x)=\left(\frac{x}{2}\right)^6$. The probability to have Si–O–Si entities with "n" oxygen atoms around the two silicon atoms, is naturally depending on the x value. For a SiO_x structured as the RBM predicts, the $P_n(x)$ is shown in figure 9.

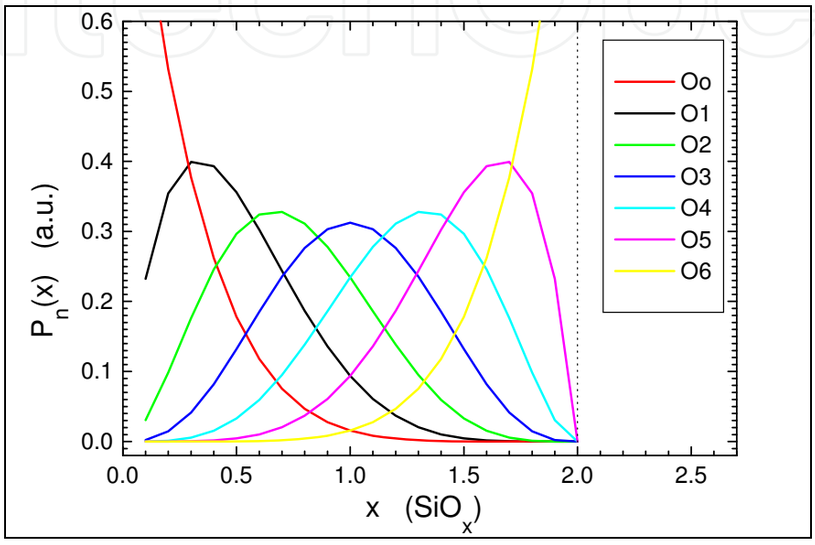

Fig. 9. The calculated probabilities to have n O-atoms bonded by Si–O-Si.

With this plot, a rough estimation of the number of the oxygen atoms and how they are bounded can be made for materials with known x parameter values. Such kind of maps are shown in figure 10 for different x values of SiO_x samples deposited via reactive sputtering. We mention that this is a theoretical estimation within the RBM approximation.

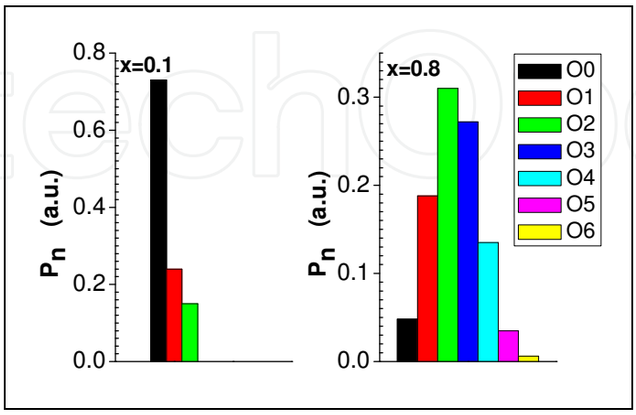

Fig. 10. The maps of the oxygen bounding probability on Si-O-Si structural bridge.

How much this model represents reality? This is a very important question for the applications of the SiO_x material and the answer will be found in the section 7.

4. Electronic density of states (DOS) in SiO_x

4.1 Introductive notions about DOS of amorphous semiconductors

In crystalline semiconductors the periodic variations of the lattice potential give rise to parabolic edges in $\vec{k}$ -space for the electronic energy bands (Ashcroft and Mermin, 1988). The conduction band is separated, in energy scale, from the valence band by the so-called "band - gap". In amorphous semiconductors there is no periodicity of the lattice. Both, the bond length and the angle between two adjacent bonds vary with small amounts around what the crystalline counterparts reveal. Considering the example of amorphous silicon, the nearest neighbors (the first coordination sphere) are the same as for the crystalline silicon, but a difference appears when we speak of near neighboring (e.g. the second coordination sphere) where deviations of about $\pm 5^o$ versus the crystallization direction appear. This gives rise to the existence of tails attached to valence- and conduction- band that penetrate into the band-gap. They are formed from localized states assigned to the carrier (electron). Generally, it is assumed that the density of states in the tail decreases exponentially into the gap.

Very often it happens that one bond is missing and the atom is sub-coordinated. Defects represented in amorphous semiconductors by "coordination defects", such as *dangling bonds,*(DB), give rise to electronic states around midgap. Dangling bonds show an amphoteric behavior, which means that a dangling bond can have three different charge states: *positively charged* when unoccupied, *neutral* when singly occupied by electron and *negatively charged* when doubly occupied. Such a defect is represented by two electronic states. There are several approaches to model the distribution of defect states within the gap of amorphous material. A standard model for the defect-state distribution assumes two symmetrical Gaussian distributions separated by the so-called correlation energy (Street, 1991) (see figure 11).

Normally, such a defect has one unbounded electron and electrically the defect is neutral, D^0. But according to the Pauli's rule, on the same energy level, another electron can be accommodated (with unparallel spin) and the defect will become negatively charged, D^-. The energy level of D^- , in comparison with D^0 will be raised due to electron-electron interaction. The existence of D^- defects implies the existence of positively charged defects, D^+, - dangling bonds where the electron is missing. The energy states assigned to DB are localized and they form narrow bands near the mid-gap. The Fermi level is pinned between them. Due to their electronic states placed deep into the band-gap, around Fermi level, the defects control the optical and electrical properties of the amorphous material.

It is unanimously agreed that the energy bands (valence- and conduction-band) are formed in amorphous semiconductors from extended states (their contribution to the transport phenomena is similar to the homologous states in crystalline materials) and localized states that form the tail. The delimitation between these two types of states is made by the *mobility edge* levels; this name derives from the fact that the electron mobility is higher when extended states are involved than the mobility of localized electrons (4 to 6 order of magnitude). It is important to mention that the mobility edges in disordered materials play the same role as the energy band edges in crystalline counterparts.

Structural disorder (deviations in bond length and bond angle) is represented in the density of states distribution by localized states in the bands' tails. Figure 11 shows the

representation for density of electron states, N(E), as a function of energy, E, according to the Mott and Davis model (Mott and Davis, 1979). The mobility edges of both the conduction- and valence-band are depicted by E_C and E_V respectively. The tails of these bands are considered as exponentially decaying into the band gap. In the case of bi- or multi-component amorphous alloy local variations in stoichiometry (composition) may appear. This means that the mobility edges will have a "sophisticated" spatial distribution.

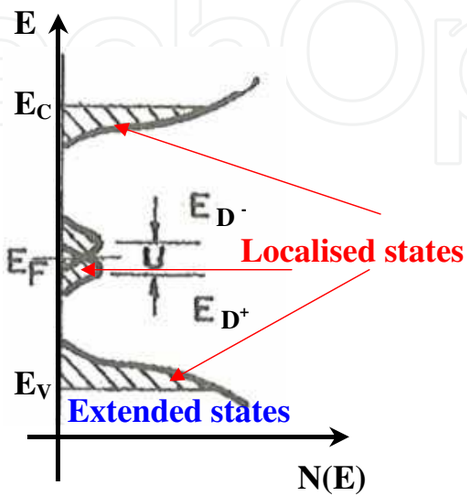

Fig. 11. Mott-Davis model for density of states (DOS) in disordered materials.

The DB density in amorphous materials depends on the quality of the material and on the technology used for layer preparation. Typical values for sputtered a-Si are 10^{19} spin/cm^3 while in SiO_x could reach 10^{22} spin/cm^3. Thermal treatment (annealing) will help relax the lattice and therefore variations in DB's have been observed. Adding hydrogen during layer deposition, the DB's density will drastically decrease. The Si-H bonding energy lies deep in the valence band (VB). Therefore, defects from mid-gap are removed through hydrogenation.

4.2 Particularities of SiO_x density of states

In the last decades, silicon suboxides have been theoretically (ab initio theories) and experimentally investigated to better understand their electronic density of states (DOS). It is well known that this parameter defines both the optical and the electrical properties of the material. According to the random bonding model of the SiO_x structure, clusters of Si_nO_m have been theoretically investigated at the quantum-mechanic level (Zhang et al., 2001a) and it was found that:

- energetically the most favorable small silicon-oxide clusters have O atomic ratios at around 0.6;
- remarkably high reactivity at the Si atoms exists in silicon suboxide Si_nO_m clusters with $2n>m$.

The total density of states (TDOS) was theoretically calculated (Zhang et al., 2001b) and projected onto the constituent atoms to deduce the contribution of the individual atoms to the total electronic structures. Such a treatment was used to find the atoms in which the

highest occupied molecular orbital – HOMO (to be assigned to the valence band edge from crystalline semiconductors) and the lowest unoccupied molecular orbital – LUMO (similar to the conduction band edge) reside. The difference LUMO-HOMO is an indication of the material band-gap. The closest molecular orbital to the gap contains a significant contribution from the Si and O atoms, as $HOMO_{Si}$, $HOMO_O$, $LUMO_{Si}$, and $LUMO_O$, respectively. In figure 12 are shown the results of the calculations as a function of the relative oxygen content into the layer. Zhang and his colleagues (Zhang et al., 2001a) have used fourth-order polynomials fit, and in figure 12 are shown $LUMO_{Si}$ (upper) and $HOMO_{Si}$ (lower) with solid curves, while dashed curves represent $LUMO_O$ (upper) and $HOMO_O$ (lower). Therefore, considering a defect-free SiO_x material, its band gap is determined by the orbital of the atomic silicon for silicon-rich material and by the orbital of atomic oxygen for silicon-poor materials. Increasing the oxygen content, the LUMO position remains at about the same energy position, while the HOMO decreases.

Taking into account the localized states induced by dangling bonds in the region of mobility band gap, the energy distribution of the density of states, can be penciled (Singh et al., 1992; van Hapert, 2002) as in figure 13. This model is inspired by the data published till 2002 and it is successfully utilized to understand the physical properties of SiO_x thin films. As main conclusions we point out:

- the conduction band is formed by Si-Si and/or Si/O antibonding states;
- the valence band is formed by Si-Si bonding states for SiO_x with $x<1.3$ and by Si-O bonding states for SiO_x with $x>1.3$;
- the silicon dangling bonds (DB) states form a band of localized electronic states at 0.7 eV below the conduction band edge.

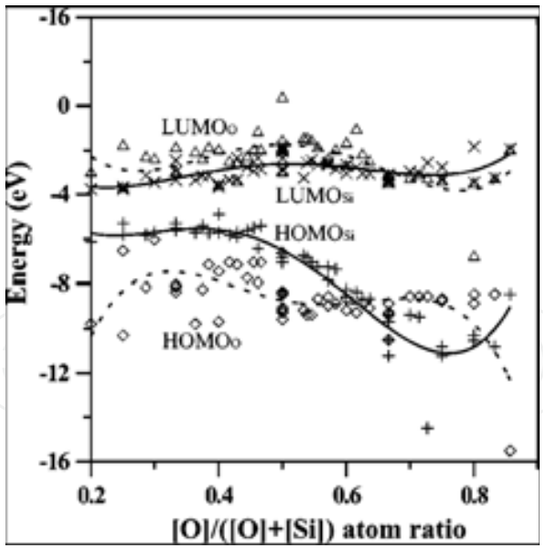

Fig. 12. Computed $LUMO_{Si}$ (×), $LUMO_O$ (Δ), $HOMO_{Si}$ (+) and $HOMO_O$ (◊) of Si_nO_m clusters. Reprinted figure with permission from Zhang et al., 2001a[2]. Copyright (2001) by American Physical Society. http://link.aps.org/abstract/PRB/v64/p113304.

[2] Zhang, R. Q.; Chu, T. S.; Cheung, H. F.; Wang, N. & Lee, S. T. Phys. Rev. B64, pp. 113304 - 113308 (2001)

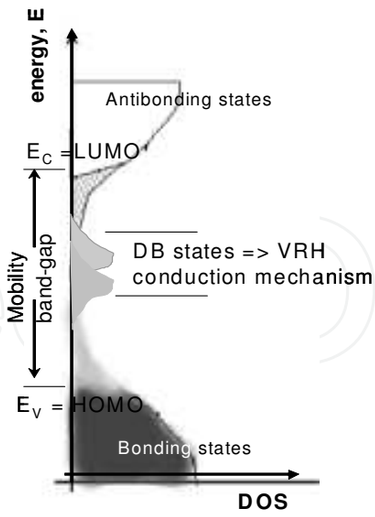

Fig. 13. Model for SiO_x density of states distribution.

4.3 The nature of the paramagnetic defects in SiO_x

In the section 4.1 it was shown that the structural defects defined by dangling bonds can be electrically neutral and positively or negatively charged. Defects' type and their density influence also the film structure. The *electron paramagnetic resonance* (EPR[3]) measurements will reveal the paramagnetic defects. These are the so-called neutral defects. Although later only this type of defects will be discussed, the presence of the positively and negatively charged defects has to be noted. These are defects with none electron or with two electrons placed on the energy level. Because of lack of the investigation methods for these defects' types, we will focus on EPR data. This technique measures the splitting of energy levels of unpaired electrons when placed in a magnetic field. The unpaired electrons essentially behave as small magnets whose orientation can be flipped by a microwave signal. The frequency at which the orientation can be flipped is determined by the strength of the applied magnetic field. This interaction between the unpaired electron and the microwave field assigned is maximized in condition of resonant oscillations of the electron. In other words, the electron absorbs energy from the microwave oscillations. The derivative absorption of microwave power is measured as a function of the magnitude of an external magnetic field. In figure 14 are shown EPR spectra of two SiO_x layers: one silicon rich, with $x=0.45$ and the other one oxygen rich sample, with $x=1.47$.

From such measurements, the important information that can be obtained is the number of paramagnetic defects and the type of these defects. The first parameter needs a standard MnO oxide sample with known number of spins. The second parameter is found by evaluating the Landée's factor (the so called g factor). For the data hereunder presented the calibration MnO sample had $3\pm1\cdot10^{15}$ spins. Comparatively to it, the paramagnetic defects' density in SiO_x layers was calculated. One has to mention that all SiO_x samples have been deposited via sputtering. The number of the EPR active defects found in SiO_x thin films as a function of layer composition (the x parameter) is shown in figure 15. As it can be seen, the

[3] The ERP measurements have been made and the results analyzed together with Dr. Ernst van Faassen at Utrecht University, The Netherlands. The fruitful discussions with him are acknowledged.

spin density is about 10^{20} cm^{-3} and increases with *x* values. For SiO_x samples with x very close to x=2, the spin density decreases.

The random distribution of the defects with various neighboring sides produces inhomogeneous line broadening. In figure 14 the differences in the plots' shape are really large when we compare the silicon rich SiO_x with the oxygen-rich one. This is related to the structural type of the paramagnetic defect. The g value will help in identification the defect type, and its values have been calculated and plotted against *x,* as figure 16 shows.

Generally, the Landée factor lies between 2.0057 – value assigned to dangling bond amorphous silicon defects (DB a-Si) and 2.001 – the value that reveals the so-called E' centers from SiO_2. Increasing the oxygen content in sample, the g values slightly decrease down to 2.004 when x varies between 0.2 and 1.2. For alloys with a larger concentration of oxygen, x>1.2, the values of the g factor steeply diminish.

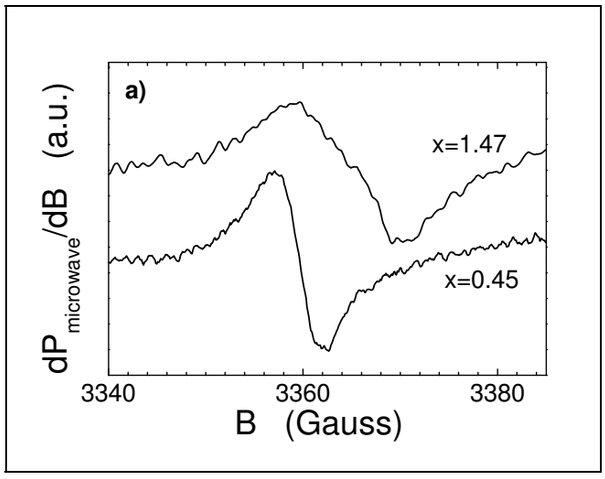

Fig. 14. Example of derivative absorption of microwave power in EPR measurements.

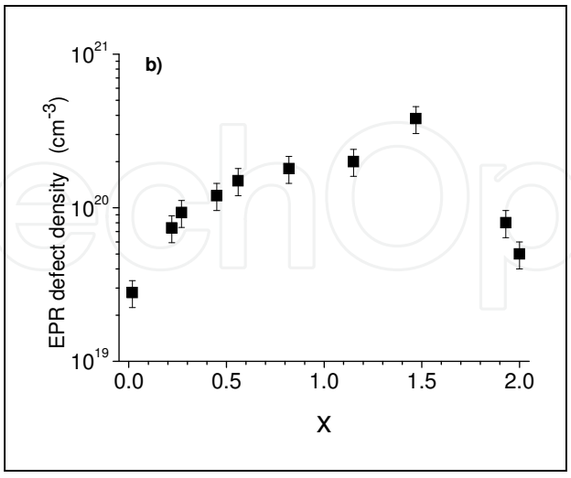

Fig. 15. The density of aramagnetic defects as a function of oxygen content in SiO_x.

In order to identify the defects types, experiments which reveal the defect saturation were carried out. The microwave magnetic field at the resonator of the EPR setup is proportional to the square root of the applied microwave power. Measuring the interaction of the spins

with the magnetic field by area of the resonant signal, a non-saturated signal is linear with $\sqrt{P}$, with P the microwave power. Studying the sample with x=1.47, at room temperature, the variation of the microwave power has emphasized two types of defects: one saturates very rapidly and the second one is practically non-saturated (see figure 17). The first type is characterized by g=2.0013 and it is identified as E' like defect, while the second has g=2.0047 and it is assigned to DB a-Si. Therefore, the a-Si dangling bonds paramagnetic defects do not saturate when the microwave power is varied up-to 30 mW, in this experiment.

No defects' saturation effect was observed for the sample with x=0.45, when the same experiment has been done. This indicates a single type of defects. According to the g-value, it is DB a-Si paramagnetic defect.

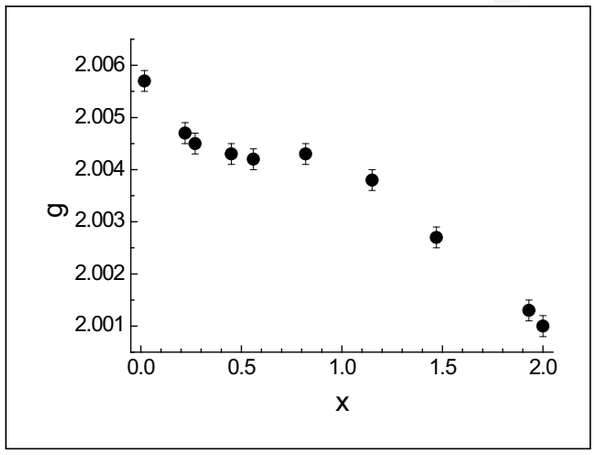

Fig. 16. The calculated values of the Landée factor is function of the oxygen content in SiO_x. In other words, the type of the paramagnetic defects is determined by the oxygen amount.

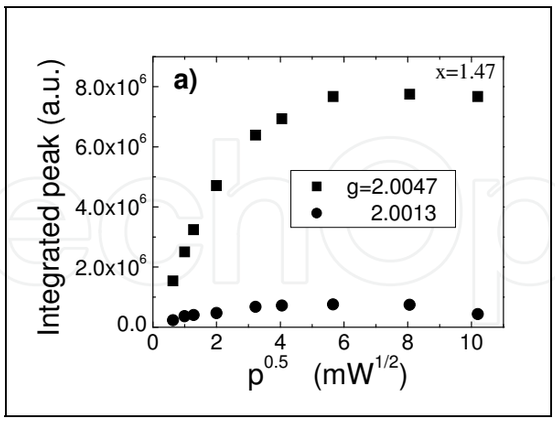

Fig. 17. The results of the saturation experiments for sample $SiO_{1.47}$. The absorption peak versus the square root of the microwave power reveals two types of paramagnetic defects in this material.

The difference between the two studied samples from this point of view is visible with the naked eyes in figure 14. The EPR registered plot for sample $SiO_{0.45}$ is sharper that that of $SiO_{1.47}$.

5. Optical properties of SiO_x thin films

5.1 Refractive and absorption index; optical band-gap

When an electromagnetic radiation interacts with a semiconductor, the optical properties of the material are revealed. If the radiation is in the UV-VIS range (the wavelength is 400 - 900 nm), the optical properties utilized to describe semiconductors are the refractive index, n, the absorption index, k, and the band-gap, E_g. We note that these physical amounts are dependent between them, according to various theories and models proposed to explain them. For example, the refractive index and the absorption index are connected between them via the Kramer-Krönig relation (Hutchings et al., 1992). Moreover, the modern theories in physics define the complex refractive index by its real part, n, and imaginary part, k, as:

$$n^*(\omega) = n(\omega) - ik(\omega) \tag{16}$$

where $\omega=2\pi\nu$ measures the electromagnetic field frequency, ν, and "i" is the unit imaginary number ($i^2= -1$).

The optical band gap, which is the separation in energy between the minimum of the conduction band and the maximum of the valence band (in other words the difference between the LUMO and the HOMO levels - see the section 4.2), can be calculated following different optical models, either from the dispersion of the refractive index n (ω), or from the spectral dependence of the absorption coefficient. In all these models, the response of the investigated material (SiO_x in our case) to the interaction with an electromagnetic wave (light) is described.

In order to reveal the optical band gap of the SiO_x, mechanisms of photon absorption are invoked. The quantum mechanic treatment of this absorption is based on, and it explains, the electronic transitions induced by the electromagnetic field in semiconductor. The main issue is the interaction between the electron belonging to the SiO_x electronic density of states and the incident photon. This interaction might have as result the transition of the electron from its initial state $\langle i|$ to a final state $|f\rangle$, transition that happens with the probability, w_{if}, given by the golden rule of the quantum mechanics:

$$w_{if} = \frac{2\pi}{\hbar}\left|\langle i|H'|f\rangle\right|^2 \delta\left(E_f - E_i - \hbar\omega\right) \tag{17}$$

In the Rel. (17), H' is the hamiltonian that describes the interaction between the electron and the electrical field assigned to the electromagnetic wave (visible light). Without getting into details (for more see Madan and Shaw, 1988) in the so-called dipole approximation, this interaction is described by:

$$H'(r,t) = q\vec{E}_0\vec{r}\cdot\exp(-i\omega t) + q\vec{E}_0\vec{r}\cdot\exp(i\omega t) \tag{18}$$

where q is the electronic charge, $\vec{E} = \vec{E}_0\exp(-i\omega t) + \vec{E}_0\exp(i\omega t)$ is the electrical field assigned to the electromagnetic wave and $\vec{r}$ is the electron displacement due to the electrical field.

With the probability of transition given by Rel. (17) and considering that for one transition the electronic system of the material absorbs energy that amounts $\hbar\omega$ - the photon energy - the absorption coefficient, α, can be calculated. By definition, α is the energy absorbed per volume unity divided to the incident flux of energy:

$$a(\omega) = \frac{\sum_{i,f} w_{if}(\omega) \cdot \hbar\omega}{(c/n)\bar{W}} \tag{19}$$

where $\bar{W} = n^2 \bar{E}_0^2$ is the averaged density of electromagnetic energy.

Introducing (17) in (19), after some calculations, following the model proposed by Tauc, Grigorovici and Vancu (Tauc et al., 1966), the absorption coefficient can be written as:

$$\alpha(\omega) \cdot (\hbar\omega)^{\xi} \approx \int_0^{\hbar\omega} g_i(-E) \cdot g_f(\hbar\omega - E) \cdot dE \tag{20}$$

with $g_i(E)$ and $g_f(E)$ as the density of electronic states for the initial and final state. The power parameter ξ can be ξ=1 when in Rel. (19) are used the momentum matrix elements, or it can be ξ= -1 when elements of the dipole matrix are used. The formula (20) is important because it helps to determine the dispersion law for the absorption coefficient. Moreover, it makes the connection between this optical parameter and the distribution of density of electronic states (see section 4). For example, when ξ=1 in the Rel. (20) and the shape of the density of states is considered parabolic, the Rel. (20) will result in the so-called Tauc fomula (Tauc et al., 1966):

$$\alpha(\omega) \cdot \hbar\omega = B \cdot (\hbar\omega - E_{gT})^2 \tag{21}$$

where E_{gT} is the "Tauc band-gap" and B is a coefficient.

On the other hand, solving in the same conditions the Rel. (20), but considering ξ= -1, the result will be the Cody formula (Cody et al., 1981), which will generate the so-called "Cody band-gap", E_{gC}:

$$\frac{\alpha(\omega)}{\hbar\omega} = C \cdot (\hbar\omega - E_{gC})^2 \tag{22}$$

with C the Cody coefficient.

From relations (21) and (22) the band gap of the semiconductor can be easily determined. However, for amorphous semiconductors there are many definitions for the optical band gap. Besides E_{gT} and E_{gC} a much utilized definition is the photon energy that corresponds to the absorption coefficient equal to 10^4 cm^{-1}, E_{04}. In the next section, we will present the so-called OJL model specially designed for amorphous materials with density of states similar to that showed in the figure 11. Up to now, it is clear that in determining the value of the optical band-gap, the dispersion of the absorption coefficient is vital.

The absorption index, k, is related to the absorption coefficient as:

$$k(\omega) = \frac{c}{2 \cdot \omega} \cdot \alpha(\omega) \tag{23a}$$

while the refractive index is correlated to the absorption coefficient via the Kramer-Krönig (Hutchings et al., 1992) relation:

$$n(\omega)-1=\frac{c}{\pi}\wp\int_0^{\infty}\frac{\alpha(\omega')}{\omega'^2-\omega^2} \tag{23b}$$

where $\wp$ denotes the Cauchy principal value.

5.2 The optical properties of the SiO_x thin films

A method to investigate the optical properties is based on the experimental measurement of the spectral transmittance and reflectance of the material. Schematically, the experiment of measuring the transmittance and the reflectance of a SiO_x thin film is shown in the figure 18. An optical radiation with intensity $\Im_0(\lambda)$ is sent on the surface of the sample. By using two spectrometers, the intensities of the reflected light, $\Im_R(\lambda)$ and that of the transmitted light, $\Im_T(\lambda)$ are measured. In this way, the reflectance $\Re(\lambda)=\Im_R(\lambda)/\Im_0(\lambda)$ and the transmittance $T(\lambda)=\Im_T(\lambda)/\Im_0(\lambda)$ are measured as a function of the utilized wavelength light. As a result of the interaction with the electronic system of the SiO_x material, part of the radiation can be absorbed by electronic excitations (intraband and/or interbands). In this way, the third physical quantity, called absorbance, A(λ), is defined[4]:

$$A(\lambda)=1-T(\lambda)-R(\lambda) \tag{24}$$

These three physical parameters are defined in terms of radiation energy.
Measuring the reflectance and the transmittance on different SiO_x samples and using the method of computer simulation proposed by Wolfgang Theiss in his Scout cod program (Theiss, 2005), the refractive and the absorption index, together with the layer thickness can be determined. In figure 19 the spectral distributions of the transmittance and reflectance measurements on SiO_x layers are shown. We mention that the thickness of the samples is around 600 nm and the changes in the shape of the spectra are due to the optical properties of the material.

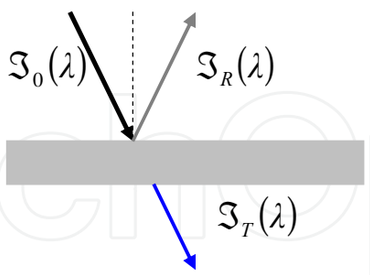

Fig. 18. When an optical radiation interacts with a solid thin film, part of it is reflected, part of it is emergent through the thin film and the rest is absorbed into the material.

The model utilized in this section to simulate the measured spectra is the so-called OJL model (O'Leary et al., 1997). The edges of the valence band and conduction band are

[4] It has to be noted that in chemistry, generally, the reflection is neglected and the absorbance is defined as: $A(\lambda)=1-\Im_T(\lambda)/\Im_0(\lambda)$

considered to be parabolic in the $\vec{k}$ space, but modulated with exponential decays. The first part (parabolic behavior) is specific to the Tauc or Cody models and they describe the extended states in both, the valence - and the conduction band. The second part (the exponential decay) represents the tails of the valence - and conduction - band formed from localized states due to the structural and compositional disorder (see figure 11 in section 4). Based on this figure, without considering the localized bands developed towards the middle of the band-gap, the definitions for the optical band gap and the DOS distribution is shown in the figure 20. Generally, the exponential tail of the valence band into the band-gap could be different than that of the conduction band ($\gamma_{VB} \neq \gamma_{CB}$). In many simulations, for simplicity and in order to have a small number of the fit parameters, they are considered equal, $\gamma_{VB} = \gamma_{CB} = \gamma$. The bigger this parameter is, the larger is the material disorder.

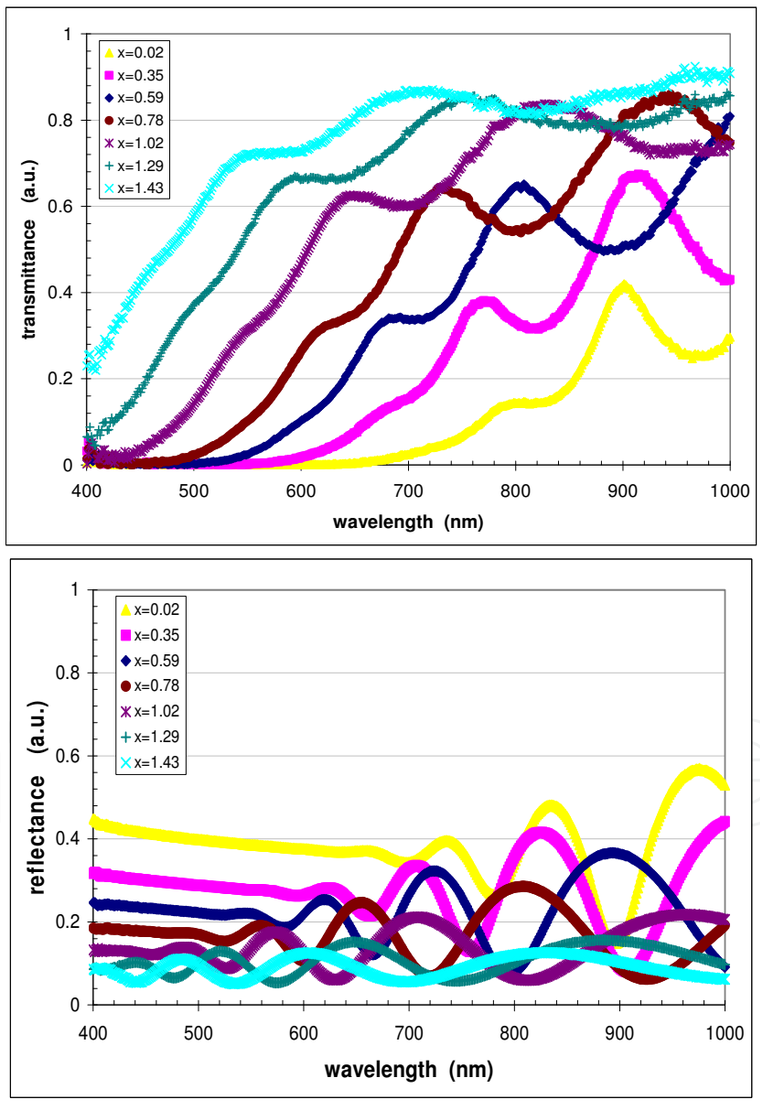

Fig. 19. The transmittance (up) and the reflectance (down) spectra of different SiO_x compositions, versus the light wavelength.

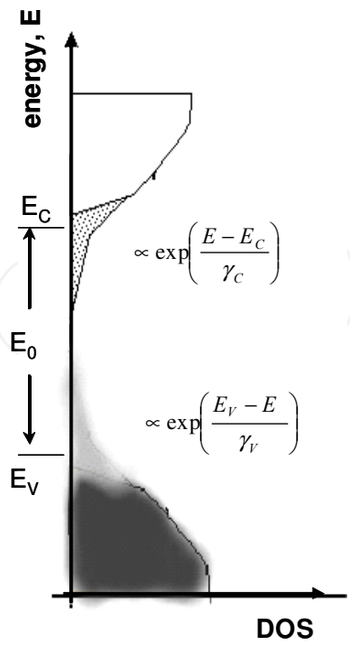

Fig. 20. The density of states for the valence band and for the conduction band in the OJL model (see the Rel. (25)). The optical band-gap, E_0 means something more than the mobility gap. The difference is made by the exponential decays of the bands' tails formed from localized electronic states.

When comparing with the density of states given in figure 13, one can see that the localized states due to the defects (placed in the center of the band gap) are mising. This is an approximation needed for an easy simulation. The DOS function describing a band structure with localized states exponentially distributed from the band edge towards the middle of the band-gap is, according to O'Leary et al., 1997:

$$g_C(E) = \frac{\sqrt{2}\cdot m_e^{3/2}}{\pi^2\hbar^3}\cdot\begin{cases}\sqrt{E-E_C} & E \geq E_C + \frac{\gamma}{2} \\ \sqrt{\frac{\gamma}{2}}\cdot\exp\left(-\frac{1}{2}\right)\cdot\exp\left(\frac{E-E_C}{\gamma}\right) & E < E_C + \frac{\gamma}{2}\end{cases}$$

$$g_V(E) = \frac{\sqrt{2}\cdot m_h^{3/2}}{\pi^2\hbar^3}\cdot\begin{cases}\sqrt{E_V-E} & E < E_V - \frac{\gamma}{2} \\ \sqrt{\frac{\gamma}{2}}\cdot\exp\left(-\frac{1}{2}\right)\cdot\exp\left(\frac{E_V-E}{\gamma}\right) & E \geq E_V - \frac{\gamma}{2}\end{cases} \quad (25)$$

where m_e, m_h is the effective mass of a charge carrier and E_C, E_V are identical to the mobility edge. The mobility band-gap is $E_0 = E_C - E_V + \gamma$. In the OJL model, the refractive index, the damping constant γ, the mobility band-gap and the thickness of the layer are parameters of the model.

As an example, the simulations of the transmittance and reflectance spectra for SiO_x with x=1.43 are shown in figure 21.

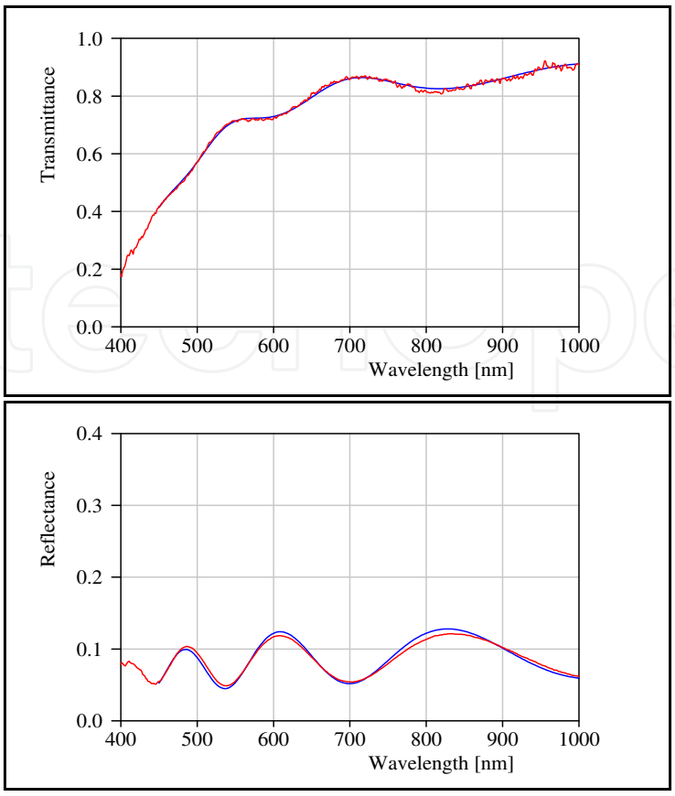

Fig. 21. The measured (in red color) and the simulated (in blue) transmittance and reflectance spectra for the $SiO_{1.43}$. The simulation was made with the Scout program using the OJL model.

The values of the fit parameters are: gamma=0.47 eV, band-gap = 2.98 eV and thickness=620.1 nm.
In a similar way the spectra of all SiO_x samples have been simulated. A curve of the refractive index versus the oxygen content can be plotted (see the figure 22).

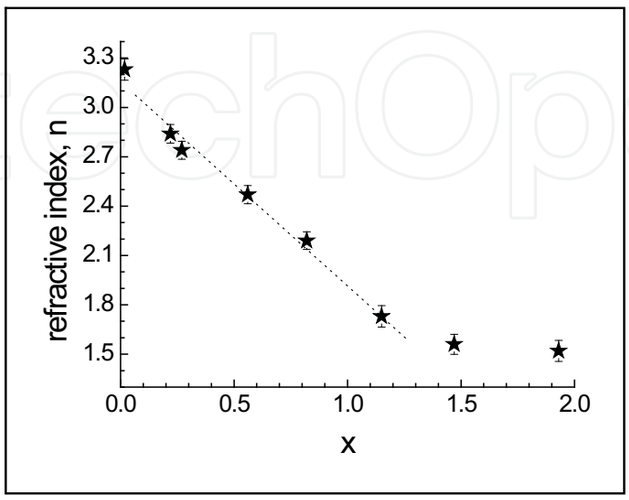

Fig. 22. The refractive index versus the oxygen content in SiO_x samples.

Increasing the oxygen content, the refractive index decreases. For x=1.3 there is a kink point, the same as the one found for the IR peak position (figure 8, section 3.3). In our opinion this is due to structural transformations that occur for highly oxygenated SiO_x layers. More on this issue, in section 7.

What about the optical band-gap determined within the OJL model? And with the Tauc band gap? These questions are answered hereunder. Because the Tauc gap needs a special representation, this question will be treated first. The absorption coefficient was calculated from the transmittance data considering the layer thickness obtained via the OJL model. According to the theory of the model presented in the previous section, the intercept with the Ox axis of the linear region of $\sqrt{\alpha \cdot \hbar\omega} = f(\hbar\omega)$ plot is the Tauc optical band-gap, E_{gT}. The modality to obtain it and, automatically the E_{gT} values are shown in the figure 23 for SiO_x samples.

Analyzing the optical-gap values plotted in figure 24, we can say that increasing the oxygen content, the band-gap increases. This is in good agreement with the trend observed for the refractive index: SiO_x with smaller refractive index is characterized by larger band-gap. This is a general feature of the semiconductor materials (Ravindra et al., 1979). Moreover, speaking of the similarities between the determined band-gap and the refractive index, a kink around x=1.3 appears. This is like a breaking in the physical properties of the SiO_x material.

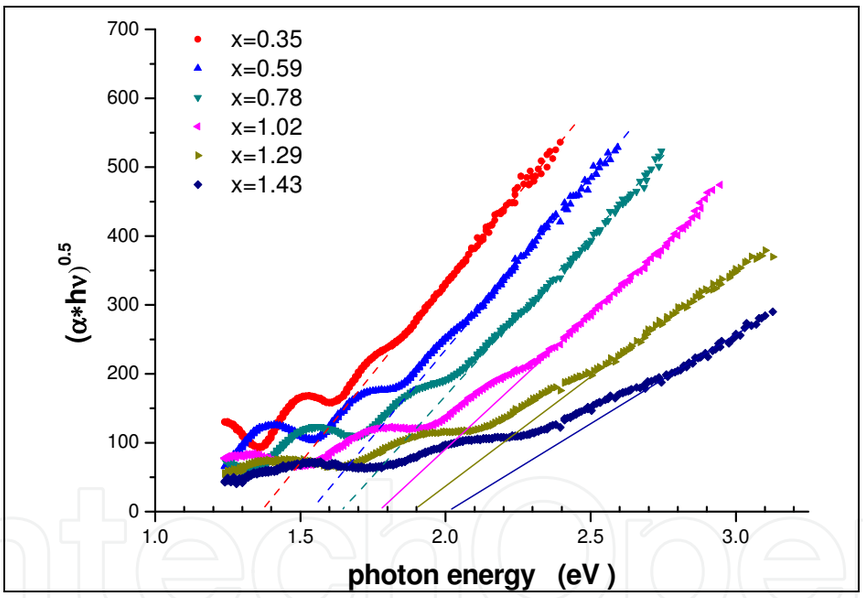

Fig. 23. The Tauc plots (see the Rel. (21)) and the corresponding Tauc band-gap values for various SiO_x layers'compositions.

The optical band-gap in the OJL model, E_0, and the exponential decay γ of the localized electronic states are obtained from simulation as fit parameters. In figure 24 these parameters are given as a function of the oxygen content.

When the variation of the γ parameter is considered, this increases with the oxygen content and the kink seems to be at x=0.6. This is not yet well understood up to now and we highlight the fact that the simulation is made considering de same decay of the localized electronic density of states for the valence band and for the conduction band, which is a strong approximation.

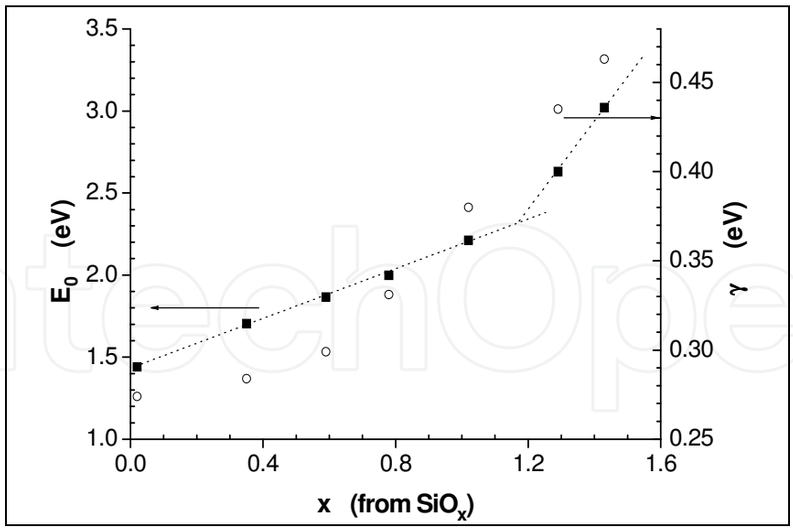

Fig. 24. The band gap, E_0 and the γ parameter that describes the exponential decay of the localized states into the band-gap, as a function of the oxygen content.

6. Electrical properties via electronic transport

6.1 Electronic transport in sputtered SiO_x

The energy and spatial distributions of the electronic density of states define the response of the material when an external electrical field is applied. The conductivity is, of course, the first electrical property that is immediately interesting for applications. A systematic research on the main conduction mechanism in SiO_x electronic transport was made by van Hapert (van Hapert, 2002). He showed that, the variable range hopping (VRH) is the theoretical model that describes better the current - voltage characteristics measured on SiO_x samples. A crucial role in understanding this mechanism is played by the localized electronic states that, spatially, are represented by the dangling bonds (DB) defects. As a function of the applied electrical field, $\vec{E}$, the electron can jump from one position to another. The hopping probability, w_{km}, between two DB sites, "k" and "m", is described by a contribution of a tunneling term and a phonon term:

$$w_{km} \sim \exp(-2\alpha\left|\vec{R}_k - \vec{R}_m\right| - \left|\varepsilon_k - \varepsilon_m\right|/k_B T) \quad (26)$$

where $\vec{R}_i$ and ε_i with i=k,m represent the position vector of the site "i" and the electron energy on that site, α is the localization parameter and k_B is Boltzmann's constant.

The hopping distance and the difference in energy between the initial state and the final state can be "chosen" such that the exponent from Rel. (26) is minimum: this is the so-called "R-ε percolation" theory. If the current-voltage characteristic has an Ohmic behavior the result of this model is the well-known Mott "$T^{-1/4}$" formula (Mott and Davis, 1979). But, for some disordered semiconductors, especially in the cases of the medium- and high-electrical field, the I-V curves become non-Ohmic. This situation has been studied within the VRH model (Brottger and Bryksin, 1985). They have defined the concept of the "directed percolation" and averaged the hopping probability as:

$$\tilde{w}\sim\exp\left(-2\alpha\cdot R+\frac{\varepsilon}{k_BT}+\frac{|e|E\cdot R}{2k_BT}\cdot\cos\theta\right) \tag{27}$$

where θ is the angle between the hopping direction $\vec{R}=\vec{R}_k-\vec{R}_m$ and the electric field, $\vec{E}$, and $\varepsilon=\varepsilon_m-\varepsilon_k$ is defined in the absence of the electrical field. Working with these assumptions, Pollak and Riess have found, for medium – and high electrical field, the current density, j, expressed as (Pollak and Riess, 1976):

$$j\sim U\cdot\exp\left[-2\alpha\cdot R_c+\frac{3}{16}\cdot\frac{E\cdot R_c}{k_BT}\right] \tag{28}$$

with R_c the critical percolation radius. Without getting too much into details, considering the electrical field E as a function of the applied voltage, it is easy to see that, in Rel. (28) the current intensity has a complicated dependence on the applied voltage. We mention that this model was successfully utilized by van Hapert to describe the SiO_x current - voltage characteristics (van Hapert, 2002).

We have to note that, in VHR, the hopping implies a DB's path that contains "returns" and "dead ends" for electrons' transfer. The carriers that arrive on the "dead ends" will have no contribution to the electrical current for that specific electrical field value. This is equivalent with a reduction of the electron density in the percolation path and an enhancement of the trapped electrons.

After this introduction into the method let's see some experimental data and how the model works. For this we propose the electrical measurements on SiO_x samples deposited via rf magnetron sputtering. The voltage has been varied between 0.01 V and 100V. A delay of 10s was considered for each experimental point between the moment of the voltage application and the current measurement. As it will be shown in the next section, for high oxygen content samples, this delay time is important.

The dc current - voltage characteristics are given in the figure 25. Every investigated SiO_x sample shows a non-Ohmic character when U>1V, ($E>2\cdot10^4$ V/cm). For these values the effect of the electrical field on the hopping processes has to be considered (see the Rel. (27)). For simplicity, the Pollak and Riess formula can be expressed in terms of experimental data (current intensity and applied voltage) as:

$$\ln\left(\frac{I}{U}\right)=a+b\cdot U \tag{28'}$$

where the slope $b=\frac{3}{16}\cdot\frac{R_C}{\delta}\cdot\frac{1}{k_BT}$ can be used to determine the reduced critical percolation path $\left(\frac{R_C}{\delta}\right)$ and the term "a" contains information about the localization parameter, α. In this expression, δ is the sample thickness that equals the distance between electrodes.

Figure 26 reveals the Pollak and Riess model applied to the investigated samples using the graphical representation inspired by the Rel. (28'). The linearity of the plots is evident and, from the slope "b" some interesting information can be obtained: a) the critical percolation path is depending on the oxygen content, as the amount and the distribution of the DB

defects; b) the silicon rich SiO_x samples are characterized by a higher conductivity and, this is consequence of less "dead ends" for carriers; c) the reduced critical percolation path, (R_c/δ), varies within about 15% when x>1.

From both, figures 25 and 26 we can observe that the SiO_x electrical conductivity is function of the applied electrical field. Also, it was already noted, the oxygen content in SiO_x plays an important role in tuning the electrical properties. Considering two representative samples - one for the silicon rich SiO_x and another one for the oxygen rich material - the calculated electrical resistance for U=50V varies from $4.15 \cdot 10^9\ \Omega$ for $SiO_{1.43}$ to $2.3 \cdot 10^4\ \Omega$ for $SiO_{0.01}$.

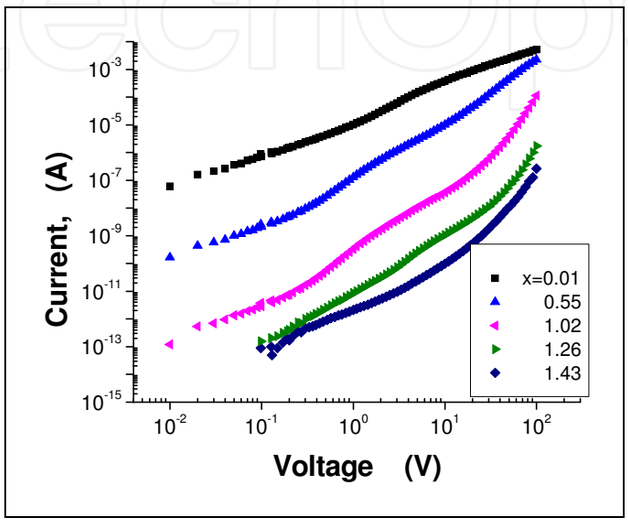

Fig. 25. The dc current-voltage characteristics measured on SiOx samples with different oxygen content. The applied voltage was varied between 0.01 V and 100 V. The non-Ohmic feature of these I -V curves is clearly revealed.

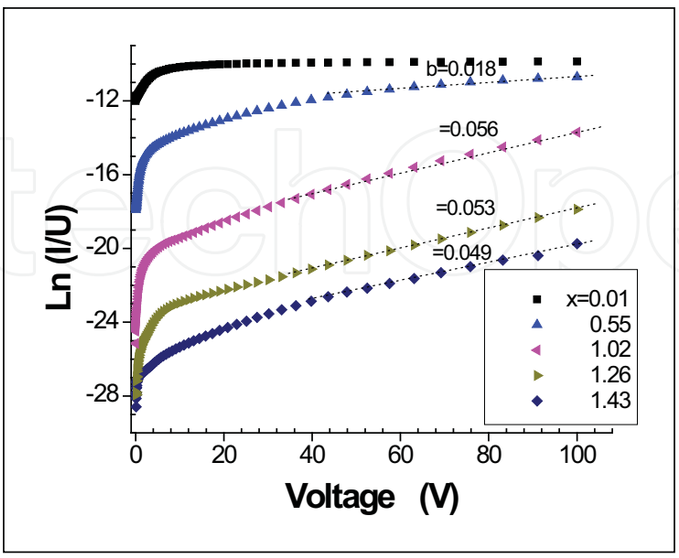

Fig. 26. The Pollak and Riess model of the VHR in current – voltage characteristics under high electrical field values is well shown for $E > 10^6$ V/cm.

6.2 Dielectric relaxation in SiO_x materials: models of investigation

The existence of the "dead ends" along the percolation path of the electrical carriers in SiO_x implies a dielectric character for the material. A "dead end" means a structural defect where one (or two) electron(s) is/are trapped a longer time than the relaxation time that defines the conductivity. This is specific to a certain electrical field value; increasing this value, the percolation path changes and the status of the "dead ends" can also change.

How can we reveal the existence of these "dead ends"? For this we propose two experiments:

a. Constant voltage pulse measurements

The application of a constant voltage pulse has the advantage that it renders the electrical field between the electrodes well known. The time variation of the electrical current through the sample gives information on the transported and trapped in "dead ends" charge carriers. In figure 27 are shown the current – time plots for the investigated samples, when a rectangular pulse voltage of 5 V was applied. For a nonzero applied voltage ($t_1<t<t_2$), the current decreases from a maximum value (determined by the voltage and the material conductivity) to a certain level that is a function of the x value. The decrease in time of the current could be easily explained if a capacitive character for the SiO_x material is considered: *the charging of this capacitor is equivalent with the diminishing of the flowing electronic flux.*

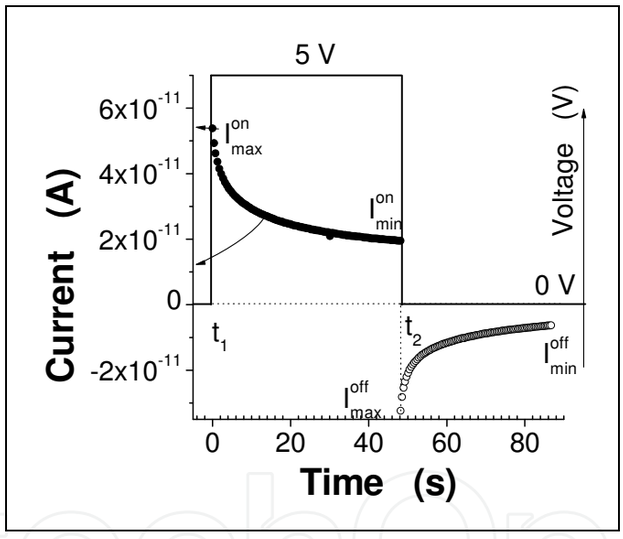

Fig. 27. The constant voltage pulse (U=5V) measurement reveals the charging of the capacitor assigned to the SiO_x through the resistor represented by the same material (the plot with full symbols). Moreover, when the voltage becomes zero at the end of the pulse, the capacitor is discharging through the same resistor (the open symbol).

From figure 27 some values of the current are of interest: the maximum and minimum values of the current through the sample during the voltage-on and voltage-off experiments. They depend, of course on the applied voltage.

When the voltage pulse is on, the measured current shows an exponential decay in time from $I^{on}_{\max}$ towards a constant value, $I^{on}_{\min}$. As we have said already, the decay reveals the capacitor charging; $I^{on}_{\min}$ is the current passing through the sample when the assigned capacitor is fully charged. The difference in electrical charges that define the $I^{on}_{\max}$ and $I^{on}_{\min}$ values is captured within the sample on the "dead ends" sites. These are silicon DB's that

can accommodate maximum two electrons and therefore becoming negatively charged. Such sites will influence the percolation path of the other electrons participating in the transport mechanism. The spatial distribution of these occupied "dead ends" has a larger density nearby the receiver electrode. We note that, the $I_{\min}^{on}$ value is depending on the x value and the applied voltage.

When the applied pulse voltage is off, as figure 27 shows, a reverse current will flow in the sample. The driving force for this current is the gradient of the fully occupied "dead ends" density. For reverse transport, these sites are not anymore "dead ends" for the charge carriers. After a while, the reverse current reaches its $I_{\min}^{off}$ value. The released charge in this time can be easily calculated by integrating the current of discharging experiments over the measurement time:

$$Q_{rel} = \int_{t_2}^{\infty} i(t) \cdot dt \tag{29}$$

In practice, the upper limit of this integral is finite to the time when $I_{\min}^{off}$ / $I_{\max}^{off}$ <10%. Considering the investigated samples with x>1, and the experimental situation when the applied voltage was U=5V, the calculated values for the charge trapped on the DB's sites distributed in the bulk of the SiO_x material are given in table 1. As a remark, increasing the amount of the oxygen in the sample, the amount of the trapped charge diminishes.

Knowing the charging voltage, V, the Q=f(V) plot reveals the layer capacity. As an example, the results for the $SiO_{1.43}$ sample are shown in figure 28. The slope of the $\log(Q_{rel})=\log(V)$ plot is 0.59. This means that the capacity is voltage dependent: $C = C_0 V^{\beta}$, with $\beta<1$ and C_0 as functions of the layer oxygen content (see the table 1). We note that increasing the oxygen content in the layer, the β parameter increases dramatically (from 0.05 for $SiO_{1.01}$ to 0.41 for $SiO_{1.43}$). The C_0 factor will be practically the voltage independent value of the capacity and is higher for the silicon richer samples. This could be macroscopically assigned to a larger value of the dielectric constant.

Of interest for applications is the dynamic of the charge releasing process from DB sites. Modeling with an exponential decay, the RC-time assigned to this phenomenon can be easily fitted. The results shown in table 1 prove that a more silicon rich sample has a smaller releasing time of the trapped charge: 1.32s for $SiO_{1.02}$ in comparison with 4.05s for $SiO_{1.43}$. These results are understandable, considering the much smaller electrical resistance of the samples with less incorporated oxygen.

x	Q_{rel} (C)	C_0 (F)	β	τ_{RC} (s)
1.02	-2.84E-09	4.26E-10	0,04	1.38
1.26	-1.50E-09	4.13E-10	0.25	2,94
1.43	-7.11E-10	1.99E-10	0.41	4.05

Table 1. The trapped charge in the so-called "dead ends", Q_{rel} , the capacity parameters (C_0 and β) and the assigned RC-time for various SiO_x samples when U=5V constant voltage pulse is applied

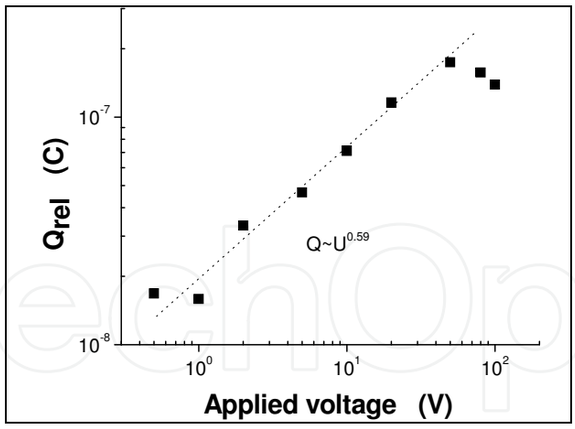

Fig. 28. Applying constant voltage pulses of different amplitude values and measuring the variation in time of the current through the sample, the chargeability of the layer can be calculated by using the Rel (29). The electrical charge versus the applied voltage defines the layer electrical capacity.

b. the hysteresis measurements

This type of measurements has been inspired by the study of the materials' magnetic properties. In fact here we apply a cycles of voltages varying in well known steps, and measure the corresponded current intensity. There is a defined delay time between applying the voltage and measuring the current. If charge is not trapped (stored) for a longer time than this delay time, the current values measured when decreasing the voltage must follow the same values as when the voltage increases. When a certain amount of charge is captured (trapped) an interesting hysteresis curve is obtained. Such an example is shown in figure 30 for two SiO_x samples: $SiO_{1.02}$ and $SiO_{1.43}$

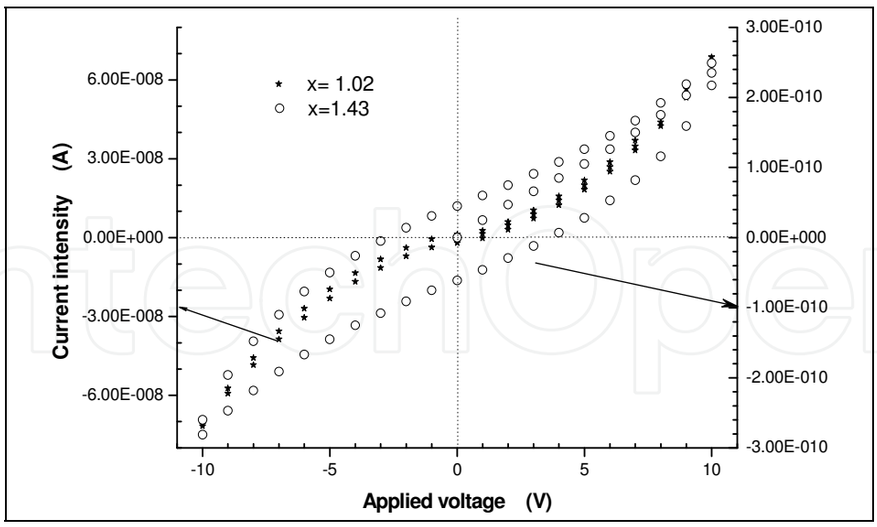

Fig. 29. The hysteresis curves current intensity versus the applied voltage for SiO_x samples with x=1.02 (full symbols) and x=1.43 (empty circles). The more resistive SiO_x showed a wider hysteresis loop.

We note the different scales for the measured current intensity through the two samples. Also, before any comment on the plots, we have to mention that the delay time between the

applying the voltage and the measuring the current was the same for both samples. The $SiO_{1.02}$ sample has a larger electrical conductivity and the hysteresis loop is narrower. Increasing the voltage, the occupation of the localized states is changed more rapidly because of the higher conductivity. When the oxygen content is increased, the material resistivity increases. The trapped charge needs more time to be released and this is well revealed by a larger hysteresis loop. During the cycle, when the current passes through zero, the voltage has a certain value, called the coercive voltage. The values for this parameter are given in the table 2. For both samples, there is an asymmetry when looking at the negative values versus the positive ones.

Sample	$U_{coercive}$ (V)		$I_{remnent}$ (A)	
$SiO_{1.02}$	-0.67	1.15	$-2.01\ 10^{-9}$	$1.18\ 10^{-9}$
$SiO_{1.43}$	-2.65	3.74	$-6.12\ 10^{-11}$	$4.56\ 10^{-11}$

Table 2. The main parameters of a hysteresis loop: the coercive voltage and the remnant current

Following the cycle in varying the voltage, we reach the situation when the voltage is null (zero), but the current intensity has a non-zero value called the remnant current. The value of this current reflects the electrical conductivity of the material, while the values of the coercive voltage is a measure of the dielectric properties. We can conclude from these experiments that the trapped charge is difficultly released from SiO_x with higher oxygen content (in the as deposited sample!).

7. From SiO_x thin films to silicon nano-crystals embedded in SiO_2

7.1 Phase separation: structural changes, thermodynamics and technology design

Most of the physico-chemical properties of a material are determined by the internal structure of that material. It is well known that models used to study the electrical, optical, thermal and magnetic properties of semiconductors are based on the density of states (DOS) distribution (electrons and/or phonons). In the last decades, many published papers emphasized the connection between the deposition conditions and the properties of the deposited SiO_x thin films. Modern and sophisticated methods of investigation revealed the structural differences for these layers.

What if a certain SiO_x material is subjected to post-deposition treatment? Is its structure changed?

For answering these questions, we review the knowledge points from section 2. The elemental structural entity in SiO_x was considered a tetrahedron with a silicon atom in the centre. The four corners of the tetrahedron are occupied by either silicon or oxygen atoms. Any type of bond is characterized by a bond energy that will define the bond length. The whole structure is formed from such tetrahedral structures interconnected. Based on calculations of the Gibbs free energy (Hamann, 2000) it was shown that tetrahedra as Si-(Si_4) and Si-(O_4) *are stable*, while Si-(Si_nO_{4-n}), with n=1, 2, 3 are *in- or unstable*. From a thermodynamics point of view the latter structures can change into a stable configuration via spinodal decomposition (van Hapert et al., 2004). The most unfavorable structural entity is Si–(Si_2O_2); the chemical bond between the central silicon atom and the oxygen ones is much stressed (disturbed) and, if conditions for migration of an oxygen atom are satisfied, the so called phase decomposition will take place. This means:

- $Si–(Si_2O_2)+ Si–(Si_2O_2)\rightarrow Si–(Si_1O_3)+ Si–(Si_3O_1)$, or
- $Si–(Si_2O_2)+ Si–(Si_2O_2)\rightarrow Si–(O_4)+ Si–(Si_4)$.

We note that the number of atoms of each species is conserved. Also, it is imperiously necessary to remark the need for intermediary structures to make the transition between the "stable" entities of amorphous silicon ($Si–(Si_4)$) and quartz ($Si–(O_4)$). In other words structures such as $Si–(Si_1O_3)$ will make the transition between the two stable structural entities.

The easiest way to check for the structural changes is to follow, by IR measurements, the peak position and the shape of the Si-O-Si stretching vibrational mode. These parameters are sensitive to the compositional and structural arrangements. We note that, in order to prove the structural changes, the experiments must be made in such a way that the composition of the layer (the x parameter from SiO_x) remains unchanged.

Without going into experimental details, as-deposited SiO_x samples have been structurally transformed by:

i. annealing (Hinds et al., 1998) at 740^0C, or
ii. ion bombardment (Arnoldbik et al., 2005), or
iii. irradiating with UV photons (mode details in the next section).

This is revealed by a new peak position that can be scaled up to the value that corresponds to SiO_2. In the figure 30 are shown some experimental results.

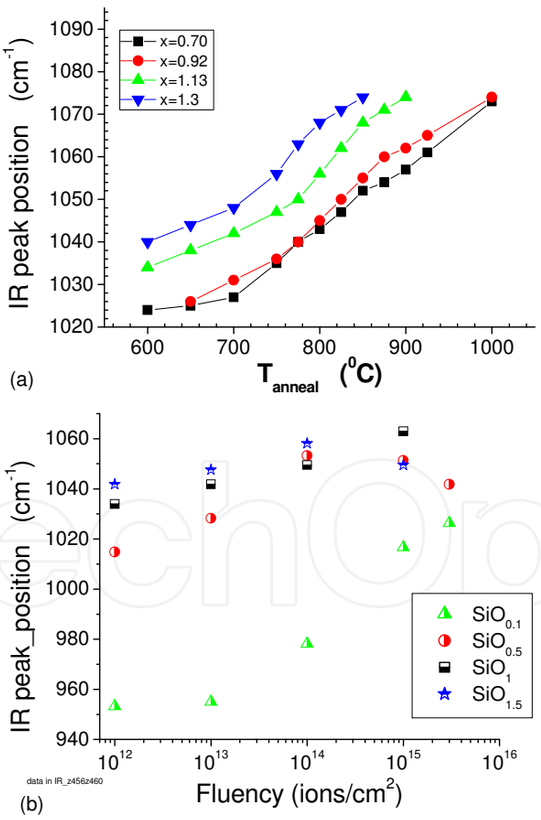

Fig. 30. The structural changes in SiO_x generated by post- deposition treatment as annealing (a) and ion bombardment (b) revealed by IR spectroscopy. The peak position of the stretching vibration is shifted towards higher wavenumber values when more energy is put into the SiO_x system. For more about this, see Hinds et al., 1998; and Arnoldbik et al., 2005, respectively.

In figure 30a it is showed that starting with SiO_x (x=0.7, 0.92, 1.13 or 1.3), via annealing at temperatures higher than 600^0C, structures where the silicon atoms are surrounded by a larger number of oxygen atoms than initially, are formed. The averaged x value remains unchanged (there are not added new atoms in the structure) but rearrangements of the oxygen atoms will provide structures characterized by a higher IR peak position. In sections 3.3 and 3.4 it was demonstrated that a larger value for the peak position means a larger x value. This applies also in these experiments: the changes in oxygen richer regions automatically mean formation of silicon rich domains. In other words the contribution of the signal assigned to the Si^{3+} and Si^{4+} sites to the total IR absorption signal is larger (see the section 3.4). We note that the Si^0 sites do not have an IR absorption signal, but they are more visible in the Raman measurements and in the XPS spectra.

The larger the annealing temperature is, the more material suffers the phase transformation and, as a consequence, the peak position is more shifted. At high temperature (T>950C) the material becomes more "oxide thermally growth" like and the peak position is shifted towards 1081 cm^{-1}, which is the position corresponding for this material.

Similar transformations can be seen in figure 30b where the experimental data are the result of the ion bombardment (50 MeV ^{63}Cu ions). This is another manner to create the conditions for phase decomposition in SiO_x. Increasing the fluency of the ions on the studied material has a similar effect as increasing the annealing temperature. The advantage on this experiment is the less time consumed, but as applicability at industrial scale it is less feasible. However for fundamental research and understanding of the processes involved, the method is valuable and highly appreciated.

As a result of the phase separation, islands of nano-crystalline silicon (Si-nc) embedded in a SiO_2 matrix are obtained. Such a structure is shown in figure 31, using a TEM spectrum (Inokuma et al., 1998). As it was proved in this section, this new material can be obtained from silicon sub-oxides SiO_x (0<x<2) as predecessors, and special post-deposition treatments.

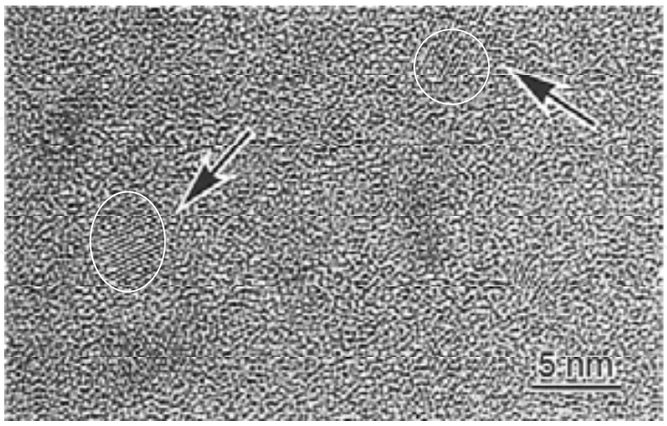

Fig. 31. Islands of Si nano-crystals embedded into a see of SiO_2 material. This new material was obtained from $SiO_{1.3}$ annealed at 1100 C. The dimension and the concentrations of these nano crystals are very important for applications in optoelectronics. *Reprinted with permission from Inokuma et al., 1998; copyright 1998, American Institute of Physics.*

7.2 Phase separation induced by UV photons irradiation

Besides annealing and ion bombardment, another post deposition technique based on laser irradiation of the SiO_x thin films has been proposed to study the phase separation process (Tomozeiu, 2006). This technique has been successfully utilized to change the structure of the various amorphous materials (carbon nitride (Zhang and Nakayama, 1997) or amorphous silicon (Aichmayr et al., 1998)). Thin films of various SiO_x compositions have been irradiated with different fluxes of UV laser photons (λ=274 nm).

In figure 32 are shown the IR spectra of the as deposited samples and of the laser irradiated samples with various amount of UV photons. The peak position of the IR stretching vibration mode measured on irradiated samples is shifted towards higher wave-number values. For a better understanding, we mention the peak position for sputter deposited SiO_2 at 1054 cm^{-1} (Tomozeiu, 2002). The as deposited $SiO_{1.2}$ samples are characterized by a peak position at 1027.7 cm^{-1}. After the laser irradiation, the main peak has its maximum at 1068.2 cm^{-1}, when the laser energy is 55 mJ (which means 103.4 mJ/mm^2). The full width at half-maximum (FWHM) - an indicator of the structural homogeneity – was also changed by UV irradiation. For the as deposited sample, the width of the peak was found 146.4 cm^{-1} and for the UV irradiated sample 106.1 cm^{-1} (55 mJ).

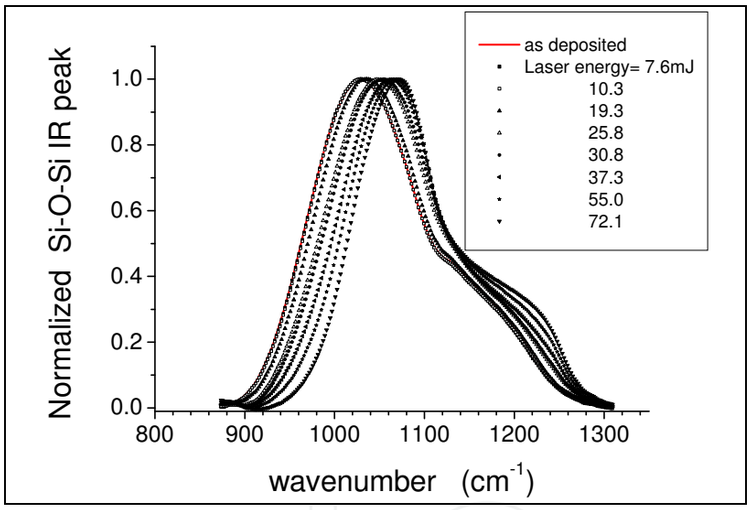

Fig. 32. The normalized IR absorption spectra of the stretching vibration mode for as deposited (full line) and UV irradiated samples with various laser energy (symbols). The energy delivered during the laser treatment is a measure of the number of the incident photons

Other issues related to the changing of the peak shape are:

i. the IR spectra of the laser treated samples have the main peak placed nearer the peak position of the thermally grown SiO_2, 1073 cm^{-1} (red shifted in comparison with the sputter deposited SiO_2;
ii. the spectrum of the irradiated sample has a shoulder at 1250 cm^{-1} that is specific to the SiO_2 structure;
iii. the shift in the peak position is dependent on the energy transferred to the SiO_x via photon impacts.

Generally, the shift in the peak position and the changes in the peak shape show the structural changes in material. Figure 33 reveals the shift in the peak position and its dependence on the incident photons' energy.

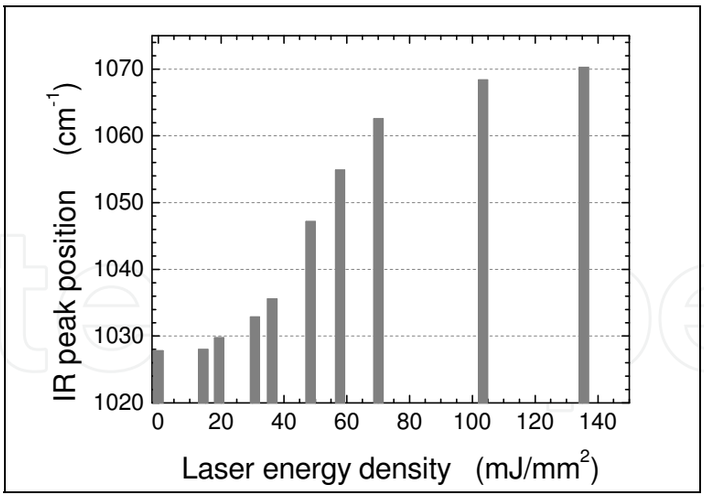

Fig. 33. The shift of the peak position assigned to the Si-O-Si stretching oscillation mode with increasing the UV photon's energy.

Considering the conservation of the silicon and oxygen atoms into the samples, the phase separation revealed by IR peak position in the figures 30 and 33 can be equated as:

$$SiO_x \rightarrow \frac{x}{2}SiO_2 + \left(1 - \frac{x}{2}\right)Si \tag{30a}$$

with intermediary steps, depending on the incident energy:

$$SiO_x \rightarrow \frac{x}{x+y}SiO_{x+y} + \left(1 - \frac{x}{x+y}\right)Si \tag{30b}$$

The peak shape is drastically changed when more energy is added in the layer, especially when the corresponding value of the SiO_x dissociation energy is exceeded. Having a calibration curve IR peak position versus oxygen content for 0<x<2 (see the section 3), the value of the y parameter can be calculated. In this way, the formation of oxygen rich regions in SiO_x can be revealed.

What about the silicon islands? Spectroscopically, they can be emphasized with Raman spectroscopy. For amorphous silicon the Raman signature is a wide peak centered on 480 cm^{-1}. If the material is crystalline, the Raman spectrum has a very sharp peak (Hayashi and Yamamoto, 1996) at 520 cm^{-1}. Figure 34 shows the Raman spectra of $SiO_{1.2}$ as deposited and laser treated samples. Increasing the laser energy, the peak centered at 480 cm^{-1} increases in intensity. This means that the amount of Si–Si bonds has been increased by the UV photon irradiation.

Therefore, IR spectroscopy revealed the increasing of the Si-O bonds' number and the Raman investigations showed the increase of the Si-Si number when the SiO_x sample has been laser irradiated. Increasing the energy delivered to the material, more oxygen-rich and silicon-rich material has been detected. Increasing more the energy delivered to the SiO_x it is possible to induce the phase separation (silicon and SiO_2) together with the phase transformation*: from amorphous into crystalline silicon*. The sharp peak centered on 520 cm^{-1}, which is the fingerprint for crystalline silicon, increases in intensity with increasing the

energy above a certain threshold value. Fitting the Raman spectrum with two gaussians – one for amorphous phase and the other for crystalline phase – the amount of the silicon transformed in crystalline silicon can be evaluated: 15.9% and 28.3% for incident UV energy of 70.1 mJ/mm^2 and 103.4 mJ/mm^2, respectively. This proves the possibilities of the method to obtain Si-nc embedded into SiO_2 matrix.

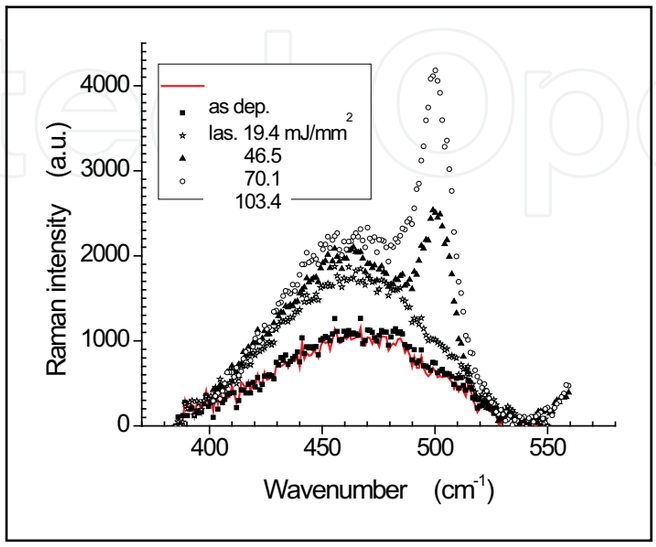

Fig. 34. The Raman spectra provide information regarding the increasing of Si-Si bonds when the photons' energy increases. The spectra of the samples irradiated with 70.1 and 103.4 mJ/mm^2 show the development of crystalline silicon from amorphous phase.

Also, the EPR measurements made on as-deposited and laser-treated samples, have revealed changes in the type of the structural defects. It was seen that, increasing the number of the incident photons, the amount of D^0 defect-like increases. Taking into account the influence of these defects on electrical conductivity, on capturing and trapping the electrical carriers and from here on the recombination electron-hole mechanisms, a real picture on the phase separation and its applicability in optoelectronics can be penciled. Such new materials as Si-nc embedded into a SiO_2 matrix (ore other dielectric matrix) are intensively studied and much required for silicon based light emitters in integrated optoelectronics.

7.3 Applications in optoelectronics

The Light Emitting Diodes (LED-s) represent together with the laser diodes the photonic devices that convert electrical energy into optical radiation. In the last half century the needs for such devices increased exponentially; new research sectors and industries have been developed due to these light producing devices. Optoelectronics, optronics and integrated optics have been developed and gained an important place in our daily life. However, as it is well known, silicon as material utilized in microelectronics devices is a poor light emitting material because of its indirect band-gap. But, silicon nano-crystals offer a solution because of their tunable indirect band-gap and more efficient electron-hole recombination. This is why, the discovery of visible light emission from silicon nano-structures has stimulated great interest for both the theoretical studies to understand the emission mechanisms, and the experimental approaches to obtain these nano-crystals. Also, the integration of such light sources within the optoelectronic devices is highly desirable.

As general knowledge, we note that the luminescence is the emission of an optical radiation due to the electronic excitation within a material. In LED the excitation of the carriers is the result of the electrical field or the current over/through the device. The photons' emission is the result of the recombination processes, which are favored by the creation of non-equilibrium states where the density of the minority carriers becomes much larger than the value corresponding to the equilibrium. We also note that within solid state devices, there are non-radiative recombination mechanisms that will reduce (cancel) the efficiency of the radiative ones.

Silicon nanocrystals can be considered low-dimensional structures with size of few nanometers. The structure of the electronic density of states is dramatically changed when theoretically we pass from three dimensional structures to one- or zero- dimensional structures. When the nanocrystals are structures with size comparable to the exciton Bohr radius (1-3 nm), the confinement induces a localization of the produced exciton. In many publications, the proposed model for the luminescence mechanisms is based on quantum confinement effects in silicon nano-crystals embedded in SiO_2 or other dielectric materials. The transition between the Si-nc and the SiO_2 matrix is a region with dangling bonds defects which appears because of the mismatch in the structural lattice of the two materials. These defects act as traps for the electrons and/or holes and, as a consequence, they quench the luminescence. Their passivation by hydrogen or oxygen atoms have been proved as being effective. According to the quantum confinement effect model, the photoluminescence in visible is observed when the band-gap of the nano-silicon is large enough due to the size reduction of the silicon nano-crystals. This together with a very well passivated surface by Si-H or Si-O bonds are the ingredients for a high efficiency in light emission from silicon nano-crystals embedded in SiO_2.

We mention that some publications suggest that surface states at the interface between the Si-nc and the composition of this intermediate layer are the principal mechanisms leading to photoluminescence Koch et al., 1993). This model opened a new perspective on approaching the emission mechanisms. Moreover, in some situations researchers invoked both models to explain the photoemissions on two different optical wavelength ranges: the emitted light at 1.8-2.1 eV is explained via the quantum confinement effects, while the band at 2.55 eV is related to localized surface states at the SiO_x/Si interface (Chen et al., 2003).

Without getting into the details of these models (this is not the purpose of this work) we consider necessary to discuss two issues: a) the influence of the nanocrystals' size on the light emission, and b) the light amplification in silicon nanocrystals.

Concerning the first subject, the spatial dimension of the silicon nanocrystals is the key factor in tuning the electronic density of states in silicon and, in the theory of the quantum confinement. Moreover the size of the nano-crystals is important in obtaining the right emission spectrum. This is revealed in figure 35 where the peak maximum of the photoluminescence is plotted against the mean crystal size according. The data are from literature (Inokuma et al, 1998; Kahler and Hofmeister, 2002) and reveal the photoluminescence (PL) spectra in SiO_x films subjected to thermal annealing between 750^0C and 1100^0C.

This study shows that there is a remarkable increase in the PL intensity after annealing at temperature above 1000^0C. Both, the composition of the as-deposited SiO_x and the annealing temperature value play an important role in the dimension of the crystals and, from here on the photoluminescence spectrum. Depending on the deposition method for the SiO_x precursor thin film and on the post-deposition treatment in order to obtain the phase

separation, the silicon nanocrystals result in different sizes. The higher is the annealing temperature, the larger are the obtained nano-crystals. From the data plotted in figure 35, a correlation between the PL peak and the mean crystal size can be penciled:

$$\lambda_{\text{PL max}}(\text{nm}) = 77.53 \cdot \text{mean cryst. size}\ (\text{nm}) + 552.6 \tag{31}$$

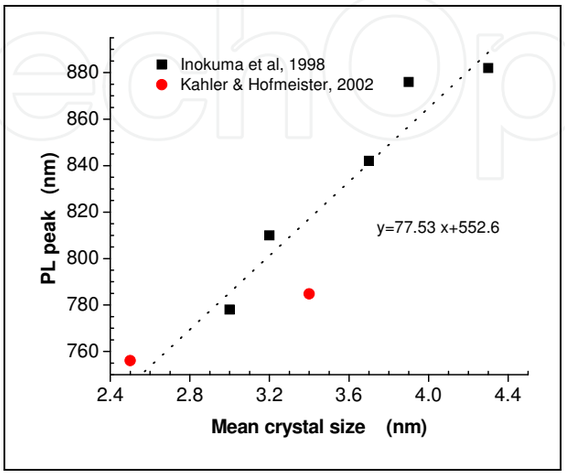

Fig. 35. The size of the silicon nanocrystals does matter in the light emission. This experimental data from literature show the importance of the post-deposition annealing in PL.

We mention that this relation was obtained from studies of SiO_x samples post-deposition annealed. Concerning the issue of silicon nanocrystals as light amplification, this is a step further from LED towards the laser diode. The works of Pavesi et al (e.g. Pavesi et al, 2000) have already penciled the main model for this new function of the silicon nanocrystals embedded into SiO_2 matrix. Their energy diagram for a nano-crystal that works in lightemission regime represents a pioneering work in this field. The diagram consists of three energy levels, where two are the HOMO and LUMO nano-crystal bands' edges and the third level is an instable energy level placed into the band-gap region (between LUMO and HOMO levels). Let it to be called inversion level. Via an external pumping mechanism the electrons are transferred from the valence band edge (HOMO level) to the conduction band edge (LUMO level) and from here, via a fast transition (time-scale of 10^{-9}s) the electrons will populate the inversion level. This is an instable energy level and the electrons will radiatively recombine with the holes from the valence band. This schematic energy diagram (see figure 7 of Pavesi et al., 2000) shows how the stimulated emission can be obtained from silicon nano-crystals embedded into SiO_2. More work is in course and we are confident that the laser light obtained from silicon-based materials, compatible with the silicon technology will be a reality in the nearest future.

In the last years, solar cells research and production have been much revigorated. Silicon based solar cells (mono-crystalline and amorphous) are the main candidates for this industry. The efficiency of a solar cell is defined by the carriers' generation per incoming photon. For photons with energy larger that the optical band-gap, it is considered that one pair of electron hole is generated by one photon. In 2000 a group of researchers at National Renewable Energy Laboratory (NREL) has found hat solar cells made with silicon nanocrystals could produce several electrons from one photon from the UV part of the

sunlight. The mechanism proposed was called "multiple exciton generation" and the calculations showed that these nanocrystals theoretically convert more than 40% of the light energy into electrical power. In a typical solar cell the energy in blue and UV light serves to produce one electron and the rest is transformed in heat. When silicon nanocrystals are used as solar cells material, this "lost" energy is converted via quantum-mechanical effects using the multiple exciton generation processes into electrons (Bullis, 2007). Although this technology is at the beginning, it is considered as the main step in obtaining a super efficient solar cell and studies are made in collecting these new generated electrons with a short lifetime.

Silicon nanocrystals are seen as promising biophotonics materials (Li and Ruckenstein, 2004; Michalet et al., 2005). In fact they can be used as luminescent markers for biological samples, having a low level of toxicity. Of great interest it is now the surface passivation of the water-dispersed Si-nc with organic compounds; in this way the luminescence is stabilized and their function as markers is more accurate. Moreover, considering the high surface-to-volume ratio of these nanocrystals, another function for them is foreseen: as therapeutic and diagnostic (theranostic) agent (Ho and Leong, 2010). There many conditions that an inorganic nanocrystal must accomplish for a complete compatibility with the *in vivo* organic material. According to this mini-review paper, the quantum dots have become a widely used research tool for diagnostics, cell and molecular biology studies and *in vivo* bioimaging. We mention that the authors have discussed only about the nano-particles as 5-50 nm of A_2B_6 (e.g. CdTe and CdSe) and A_3B_5 (e.g. InAs and InP) group of materials. A problem that must be solved is related to the toxicity of these elements for the living cell. It seems that the silicon nanocrystals are characterized by a low toxicity level and their use for these applications is in study.

As it was seen from this section the applications for the silicon nanocrystals embedded into a dielectric matrix are multiple and very actual. A better understanding of the processes that enable their formation and growth, and of their role within an optoelectronic (of biophotonic) application will end up into a high quality and more efficient devices.

8. Acknowledgements

The author is grateful to the group headed by Prof. Dr. FHPM Habraken from Utrecht University for support and interesting discussions. The permanent support offered by R&D Océ Technologies B.V. is acknowledged.

9. Reference

Aichmayr, G.; Toet, D.; Mulato, M.; Santos, P.V.; Spangenberg, A.; Christiansen, S.; Albrecht, M. & Strunk, H.P., (1998), *Lateral grain growth during the laser interference crystrallization of a-Si,* Phys. Status Solidi, A166, pp. 659 - 666.

Arnoldbik, W.M.; Tomozeiu, N.; van Hattum, E.D.; Lof, R.W.; Vredenberg, A.M. & Habraken, F.H.P.M., (2005), *High-energy ion-beam-induced phase separation in SiO_x films,* Phys. Rev. B71, pp. 125329-125336

Ashcroft , N.W. & Mermin, N.D. (1988). *Solid State Physics*, ISBN0-03-049346-3, ch. 17

Brottger, H. & Bryksin, V.V. (1985). *Hopping conduction in solids*, Akademie-Verlag Berlin, ISBN-10 -_0895734818, pp. 236

Bullis, K. (2007), *Silicon Nanocrystals for Superefficient Solar Cells* paper published on 15

Augusts 2007, in http://www.technologyreview.com

Carrier, P;. Abramovici, G.; Lewis, L.J. & Dharma-Wardana, M.W.C. (2001). *Electronic and Optical Properties of Si/SiO_2 Superlattices from First Principles : Role of Interfaces.* Mat. Res. Soc. Symp. Proc. vol. 677, pp. AA4.10.1 - AA4.10.6

Carrier, P.; Lewis, L.J. & Dharma-Wardana, M.W.C. (2002). *Optical properties of structurally relaxed Si/SiO_2 superlattices: The role of bonding at interfaces,* Phys. Rev. B65, pp. 165339-165350

Chen, X.Y.; Lu, Y.F.; Wu, Y.H.; Cho, B.J.; Liu, M.H.; Dai, D.Y. & Song, W.D. (2003), *Laser annealing of silicon nanocrystal films prepared by pulsed-laser deposition,* J. of Appl. Phys. 93, no.10, pp. 6311 - 6316

Cho, K.S.; Park, N-M.; Kim, T-Y.; Kim, K-H.; Sung, G. Y. & Shin, J. H. (2005), *High effieciency visible electroluminescence from silicon nanocrystals embedded in silicon nitride using a transparent doping layer,* Appl. Phys. Lett. 86, pp.909-071911

Cody, G. D.; Tiedje, T.; Abeles, B.; Brooks, B. & Goldstein, Y. (1981*). Disorder and the Optical-Absorption Edge of Hydrogenated Amorphous Silicon,* Phys. Rev. Lett. 47, pp. 1480-1483

Cullis, A.G. & Canham, L.T. (1991). *Visible light emission due to quantum size effects in highly porous crystalline silicon,* Nature 353 pp. 335-338

Gibbs, G.V.; Boisen, M.B.; Hill, F.C.; Tamada, O. & Downs, R.T. (1998). *SiO and GeO bonded interactions as inferred from the bond critical point properties of electron density distributions,* Phys Chem Minerals 25, 574-584

Hamann, D.R., (2000), Energetics of silicon suboxides, Phys. Rev., B61 pp.9899-9901

Hayashi, S. & Yamamoto, K. (1996) *Optical properties of Si-rich SiO_2 films in relation with embedded Si mesoscopic particles,* J. Lumin. 70 no. 1-6, pp. 352 - 363.

Hinds, B.; Wang, F.; Wolfe, D.; Hinkle, C. & Lucovsky, G. (1998), *Investigation of postoxidation thermal treatments of Si/SiO_2 interface in relationship to the kinetics of amorphous Si suboxide decomposition,* J. Vac. Sci. Technol. B16, pp. 2171-2177

Ho, Y.P. & Leong, K.W. (2010), *Quantum dot-based theranostics,* Nanoscale, 2, pp. 60 -68

Hutchings, D.C.; Sheik-Bahae, M.; Hagan, D.J. & van Stryland, E.W. (1992). *Kramers-Kronig Relations in Nonlinear Optics,* Optical and Quantum Electronics 24 , pp. 1-30 (and the first two references of this paper)

Inokuma, T.; Wakayama, Y.; Muramoto, T.; Aoki, R.; Kurata, Y. & Hasegawa, S. (1998), *Optical properties of Si clusters and Si nanocrystallites in high-temperature annealed SiOx films,* J.of Appl. Phys. 83, nr 4, pp. 2228 - 2234

Kahler U. & Hofmeister, H. (2002), *Size evolution of silicon nanocrystallites in evaporated thin films of SiO_x upon thermal processing*, Appl. Phys. A74, pp. 13 - 17

Knights, J.C.; Street, R.A. & Lucovsky, G. (1980). *Electronic and structural properties of plasma-deposited a-Si:O:H - The story of O_2,* J. Non-Cryst. Solids, 35-36 pp. 279 - 284

Koch, F.; Petrova-Koch, V. & Muschik, T. (1993), *The luminescence of porous Si: the case for the surface state mechanism*, J. of Luminescence 57, pp. 271 - 281

Li, Z.F. & Ruckenstein, E. (2004), Water-soluble poly(acrylic acid) grafted luminescent silicon nanoparticles and *t*heir *u*se as *f*luorescent *b*iological *s*taining *l*abels , Nano Letters, 4, no. 8, pp. 1463 -1467

Lu, Z.H.; Lockwood, D.J. & Baribeau, J.M. (1995). *Quantum confinement and light emission in SiO_2/Si superlattices,* Nature 378, pp. 258-260

Lucovsky, G. & Pollard, W.B. (1983). *Local bonding of oxygen and hydrogen in a-Si:H:O thin films,* J. Vac. Sci. Technol. A 1, pp. 313 - 317

Madan, A. & Shaw, M. (1988). *The physics and applications of amorphous semiconductors*, Academic Press Inc. ISBN-10: 9780124649606

Michalet, X.; Pinaud, F.F.; Bentolila, L.A.; Tsay, J.M.; Doose, S.; Li, J.J.; Sundaresan, G.; Wu, A.M.; Gambhir,S.S. & Weiss, S. (2005), *Quantum Dots for Live Cells, in Vivo Imaging, and Diagnostics,* Science, 307, no 5709, pp. 538-544

Morimoto, A.; Nariyama, H. & Shimizu ,T. (1987). *Structure and Defects in Amorphous Si–O Films,* Jap. J. of Applied Phys. 26, no. 1, pp. 22-27

Mott, N.F. & Davis, E.A. (1979). *Electronic processes in non-crystalline materials*, Oxford University Press, second edition, ch 2

Nassiopoulos, A.G.; Grigoropoulos, S. & Papadimitriou, D. (1996). *Electroluminescent device based on silicon nanopilars,* Appl. Phys. Lett. 69, pp. 2267-2269

O'Leary, S.K.; Johnson, S.R. & Lim, P.K. (1997). *The relationship between the distribution of electronic states and the optical absorption spectrum of an amorphous semiconductor: An empirical analysis,* J. Appl. Phys., 82, no 7, pp. 3334 - 3341

Pai, P.G.; Chao, S.S.; Takagi, Y. & Lucovsky, G. (1986). *Infrared spectroscopic study of SiOx films produced by plasma enhanced chemical vapor deposition*, J. Vac. Sci. Technol. A 4 (3), pp. 689-695

Pavesi, L.; Dal Negro, L;. Mazzoleni, C.; Franzo, G.& Priolo, F. (2000). *Optical gain in silicon nanocrystals*, Nature 408, pp. 440-444

Pollak, M. & Reiss, I. (1976). A percolation treatment of high-field hopping transport , J. Phys. C 9 pp. 2339 - 2352

Puzder, A.; Williamson, A. J.; Crossman, J. C.; & Galli, G. (2002). *Surface Chemistry of Silicon Nanoclusters*, Phys. Rev. Lett. 88, pp. 097401 - 04

Ravindra, N.M.; Auluck, S. & Srivastava, V. K. (1979). On the Penn gap in semiconductors, Phy. Stat. Sol B 93, no. 2, pp. K155 - K160

Singh, A.; Bayliss, S.C.; Gurman, S.J. & Davis, E.A. (1992), *The amorphous SiO_x: H_y thin film system. III. Structure and bonding*, J. Non-Cryst. Solids 142, pp. 113 - 125

Stolze, F.; Zacharias, M.; Schippel, S. & Garke, B. (1993). *Compositional investigation of sputtered amorphous SiOX*:H, Solid State Communications, 87, no. 9 pp. 805-808

Street, R.A. (1991). *Hydrogenated amorphous silicon*, Cambridge University Press, ch. 4.

Tauc, J.; Grigorovici, R. & Vancu, A. (1966*). Optical Properties and Electronic Structure of Amorphous Germanium,* Phys. Stat. Sol. 15, pp. 627- 637

Theiss,W. (2002). Scout program in *http://www.wtheiss.com*

Tomozeiu, N.; van Hapert, J.J.; van Faassen, E.E.; Arnoldbik, W.M.; Vredenberg, A.M. & Habraken, F. H. P. M. (2002), *Structural properties of a-SiOx layers deposited by reactive sputtereing technique,* J. of Optoelectronics and Advance Materials, 4, no. 3, pp. 513 - 521

Tomozeiu, N.; van Faassen, E.E.; Habraken, F.H.P.M. (2003). *Structural transition in silicon suboxides at critical oxygen content,* Annals of West University of Timisoara, Series Chemistry 12, no. 3, pp 1039 - 1046

Tomozeiu, N. (2006), *Effects of UV photon irradiation on SiOx (0<x<2) structural properties,* Applied Surface Science 253, pp. 376–380

Tomozeiu, N. (2006). *SiOx, thin films deposited by rf magnetron reactive sputtering: structural properties designed by deposition conditions,* J. of Optoelectronics and Advance Material, 8, no. 2 pp. 769 -775

van Hapert, J.J. (2002). *Hopping conduction and chemical structure - a study on silicon suboxides,* PhD Thesis, Utrecht University ISBN 90-393-3063-8, ch 3 and 4

van Hapert, J.J.; Vredenberg, A.M.; van Faassen, E.E.; Tomozeiu, N.; Arnoldbik, W.M. & Habraken, F. H. P. M., (2004), *Role of spinodal decomposition in the structure of SiOx* , Phys. Rev. B 69 pp. 245202-245210

Zacharias, M.; Drusedau, T.; Panckow, A.; Freistedt, H. & Garke, B. (1994). *Physical properties of a-SiOx : H alloys prepared by dc magnetron sputtering with water vapour as oxygen source,* J. of Non-Crystalline Solids 169, pp. 29-36

Zhang, M. & Nakayama, Y. (1997), *Effect of Ultraviolet Light lrradiation on Amorphous Carbon Nitride Films,* J. Appl. Phys. 82, no. 10, pp. 4912- 4015.

Zhang, R. Q.; Chu, T. S.; Cheung, H. F.; Wang, N. & Lee, S. T. (2001). *High reactivity of silicon suboxide clusters,* Phys. Rev. B64, pp. 113304 - 113308

Zhang, R. Q.; Lee, C. S. & Lee, S. T. (2001). The electronic structures and properties of Alq3 and NPB molecules in organic light emitting devices: decompositions of density of states J. Chem. Phys. 112, pp. 8614-8620

Weast, R.C. (1968). editor of *Handbook of Chemistry and Physics*, the 48-th edition, The Chemical Rubber Publishing Co., F149

Wilson, W.L.; Szajowski, P.F. & Brus, L.E. (1993). *Quantum Confinement in Size-Selected, Surface-Oxidized Silicon Nanocrystals,* Science 262, pp. 1242-1244

Wolkin, M.V.; Jorne, J.; Fauchet, P.M. Allan, G. & Delerue, C. (1999). *Electronic states and luminiscence in porous silicon quantum dots*, Phys. Rev. Lett. 82, pp. 197-200

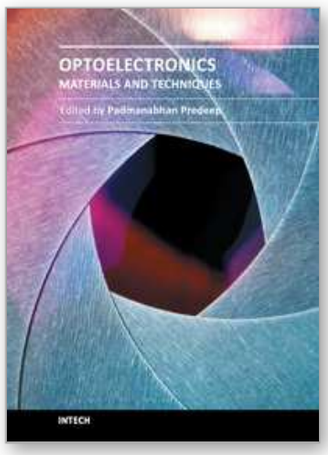

Optoelectronics - Materials and Techniques

Edited by Prof. P. Predeep

ISBN 978-953-307-276-0
Hard cover, 484 pages
Publisher InTech
Published online 26, September, 2011
Published in print edition September, 2011

Optoelectronics - Materials and Techniques is the first part of an edited anthology on the multifaceted areas of optoelectronics by a selected group of authors including promising novices to the experts in the field. Photonics and optoelectronics are making an impact multiple times the semiconductor revolution made on the quality of our life. In telecommunication, entertainment devices, computational techniques, clean energy harvesting, medical instrumentation, materials and device characterization and scores of other areas of R&D the science of optics and electronics get coupled by fine technology advances to make incredibly large strides. The technology of light has advanced to a stage where disciplines sans boundaries are finding it indispensable. Smart materials and devices are fast emerging and being tested and applications developed in an unimaginable pace and speed. Here has been made an attempt to capture some of the materials and techniques and underlying physical and technical phenomena that make such developments possible through some real time players in the field contributing their work and this is sure to make this collection of essays extremely useful to students and other stake holders such as researchers and materials scientists in the area of optoelectronics.

InTech Europe
University Campus STeP Ri
Slavka Krautzeka 83/A
51000 Rijeka, Croatia
Phone: +385 (51) 770 447
Fax: +385 (51) 686 166
www.intechopen.com

InTech China
Unit 405, Office Block, Hotel Equatorial Shanghai
No.65, Yan An Road (West), Shanghai, 200040, China
中国上海市延安西路65号上海国际贵都大饭店办公楼405单元
Phone: +86-21-62489820
Fax: +86-21-62489821

IntechOpen